Control of preexisting faults on geometry and kinematics in the northernmost part of the Jura fold-and-thrust belt

Kamil Ustaszewski[1] and Stefan M. Schmid[1]

Received 20 October 2005; accepted 30 May 2006; published 27 September 2006.

[1] This study investigates the formation of the northernmost anticlines of the late Miocene to early Pliocene thin-skinned Jura fold-and-thrust belt and provides evidence that a transition to thick-skinned tectonics did occur in this particular area during the late Pliocene. The northernmost anticlines of the Jura fold-and-thrust belt are characterized by pronounced along-strike asymmetries that were predetermined by a fault pattern inherited from Paleogene Upper Rhine Graben rifting. This fault pattern had disrupted the Triassic basal décollement of the Jura Mountains and controlled the nucleation of thrusts and folds, as well as transfer zones during the generally (N)NW directed transport of the detached sedimentary cover. Sinistral, transpressive oblique ramps nucleated along Paleogene, NNE trending basement normal faults and led to a northward protrusion of the Jura front, encroaching onto the southernmost Upper Rhine Graben. Shortening across the frontal anticlines is greatest along the oblique ramps and decreases along strike toward the east, necessitating a gentle clockwise rotation of the detached sediments. Despite the fact that the stress field in the sedimentary cover remained unchanged, thin-skinned folding and thrusting came to a halt in the early Pliocene, giving way to thick-skinned tectonics, very probably governing neotectonic activity in the area. This transition might represent a geodynamic reorganization of the northwestern Alpine foreland.
Citation: Ustaszewski, K., and S. M. Schmid (2006), Control of preexisting faults on geometry and kinematics in the northernmost part of the Jura fold-and-thrust belt, *Tectonics*, *25*, TC5003, doi:10.1029/2005TC001915.

1. Introduction

1.1. Research Objectives

[2] The present-day architecture of the northwestern Alpine foreland is largely the result of an interplay between extensional and compressional tectonics that took place since the early Cenozoic [*Dèzes et al.*, 2004]. Resulting interferences are particularly complex in the northern Jura fold-and-thrust belt (detached Mesozoic of Figure 1), where the southern Upper Rhine Graben (URG), formed during Eocene to Oligocene extension, abuts the northernmost folded Jura, formed in response to collision in the Alps during late Miocene to early Pliocene times (Figure 1). The geometry of the northern Jura fold-and-thrust belt was strongly controlled by differently oriented basement-rooted extensional faults inherited from Paleogene rifting. They not only dissected the décollement horizon to become active later during thin-skinned Jura tectonics [*Laubscher*, 1961, 1987], but also were often reactivated in compression and/or transtension before, during and after the late Miocene décollement of the cover series [*Giamboni et al.*, 2004; *Ustaszewski et al.*, 2005b]. This study contributes to the understanding of the control of such preexisting faults and their reactivation by presenting a detailed case study from the northernmost part of the folded Jura Mountains. Emphasis is given to the kinematics of preexisting faults in both basement and sedimentary cover by integrating the following data sets: (1) new field observations and paleostress analyses, (2) new compilations of subsurface maps based on existing industry seismic reflection lines, (3) published geological maps, and (4) newly constructed cross sections. After an introduction to the geological setting, outcrop-scale evidence for fault reactivation during thin-skinned Jura folding and appropriate crosscutting relationships are presented. Paleostress orientations, derived from the collected fault slip data, including timing constraints for these deformations, are provided next. On the basis of geological cross sections and geometric considerations, a kinematic model for the formation of the northern Jura folds is proposed, highlighting the influence of inherited faults. Eventually, possible reasons for the cessation of décollement tectonics during the early Pliocene and the subsequent transition to thick-skinned tectonics, very probably governing neotectonic activity in the area [*Giamboni et al.*, 2004; *Ustaszewski et al.*, 2005b], are discussed.

1.2. Geological Setting

[3] The arc-shaped, northwest verging fold-and-thrust belt of the Jura Mountains forms the most external part of the central and western Alpine orogen (Figure 1 inset). Branching off from the western Alps near Chambéry, it extends along strike over a distance of some 300 km to the northwest of Zürich [*Philippe et al.*, 1996; *Affolter and Gratier*, 2004]. It is separated from the central Alps by the Molasse Basin, a flexural foreland basin that developed in response to the load of the NW-ward advancing Alpine orogen during the Oligocene to Miocene. In the west and north, the Jura Mountains encroach onto the north to NNE

[1]Geologisch-Paläontologisches Institut, University Basel, Basel, Switzerland.

0278-7407/06/2005TC001915$12.00

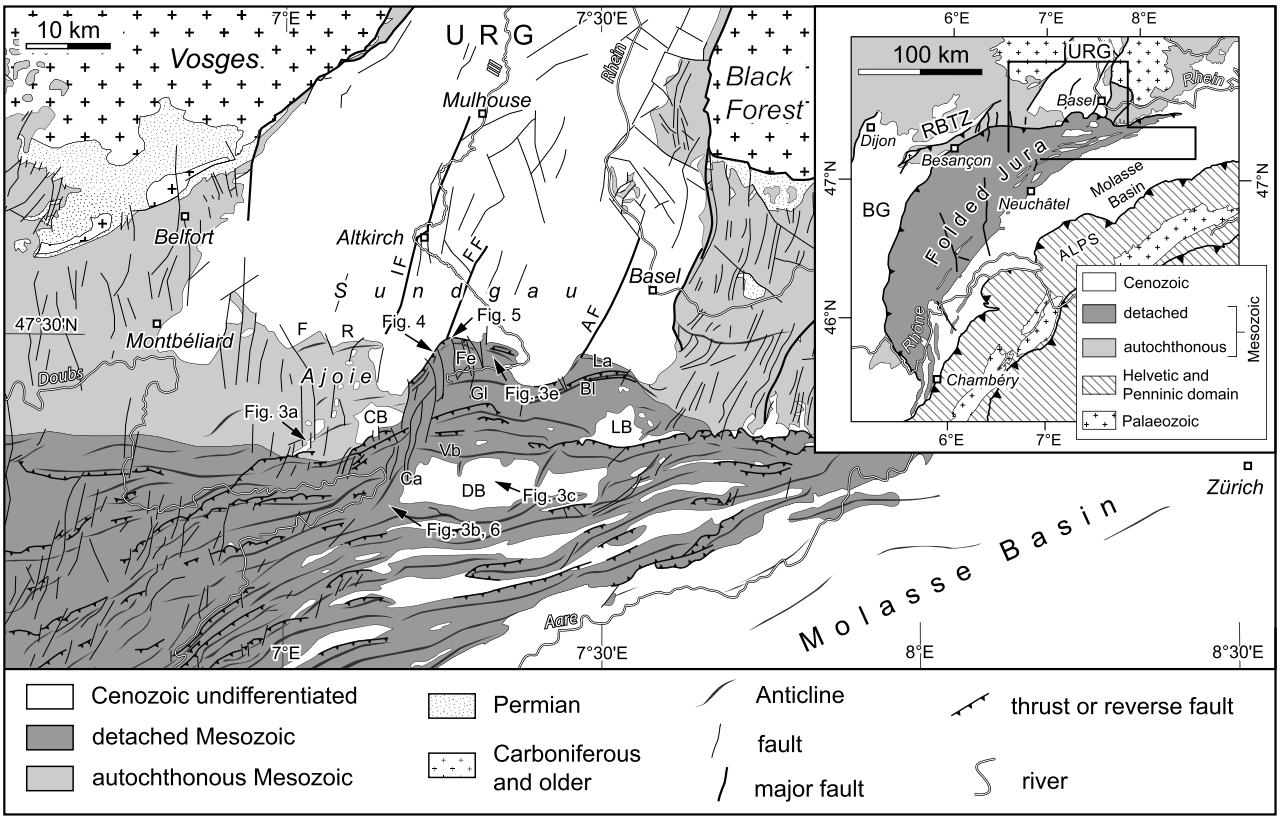

Figure 1. Tectonic map of the northern Jura fold-and-thrust belt, showing names mentioned in this study. Geographic names are in italics. Locations of Figures 3 to 6 are also indicated. Abbreviations are AF, Allschwil fault; Bl, Blauen anticline; Ca, Caquerelle anticline; CB, Charmoille basin; DB, Delémont basin; F, Florimont anticline; Fe, Ferrette anticline; FF, Ferrette fault; Gl, Glaserberg anticline; IF, Illfurth fault; La, Landskron anticline; LB, Laufen basin; Vb, Vorbourg anticline. In this study, the term "Ferrette Jura" refers to the entire frontal segment of the fold-and-thrust belt, whereas "Ferrette anticline" only refers to its frontal arc-shaped anticline. Note the conspicuous north directed protrusion of the folded Jura front along NNE trending faults of the URG system. Inset shows tectonic position of the Jura belt between the Alps and the European Cenozoic rift system. Abbreviations are Bes, Besançon; BG, Bresse Graben; RBTZ, Rhein-Bresse transfer zone; URG, Upper Rhine Graben.

trending Bresse Graben and Upper Rhine Graben (URG), which are parts of the European Cenozoic rift system [*Ziegler*, 1992] that essentially formed during the late Eocene to Oligocene. Bresse Graben and URG are separated by the Rhine-Bresse transfer zone (RBTZ), which linked simultaneous openings by sinistral transtensive movements. The location of the RBTZ was largely controlled by preexisting, NE to ENE trending faults inherited from late Variscan times [*Laubscher*, 1986; *Ziegler*, 1992; *Schumacher*, 2002; *Ustaszewski et al.*, 2005a]. The development of the Bresse Graben and URG in the northern Alpine foreland was, in a broad sense, contemporaneous with the collision phases of the Alpine and Pyrenean orogenies [*Dèzes et al.*, 2004]. The URG in particular forms the most conspicuous part of the European Cenozoic rift system, extending over a length of some 300 km from the Rhenish Massif in the north to the Jura Mountains in the south and with an average width of 30 to 40 km. While subsidence in the northern part of the URG was continuous up to the Plio-Pleistocene, it has come to a halt in the southern part in the early Aquitanian (Figure 2). This cessation of subsidence was caused by widespread uplift of the Vosges–Black Forest arch. The development of this arch, which entailed uplift of the southern parts of the URG and a truncation of its sedimentary infill, was attributed either to the northward migration of the flexural forebulge of the Alps [*Laubscher*, 1992] or to large-scale lithospheric folding in response to the buildup of a NW directed stress field that increased collisional coupling between the Alps and their northern foreland [*Ziegler et al.*, 2004]. From early Miocene times onward, the southern URG thus became part of the northwestern Alpine foreland and has since then

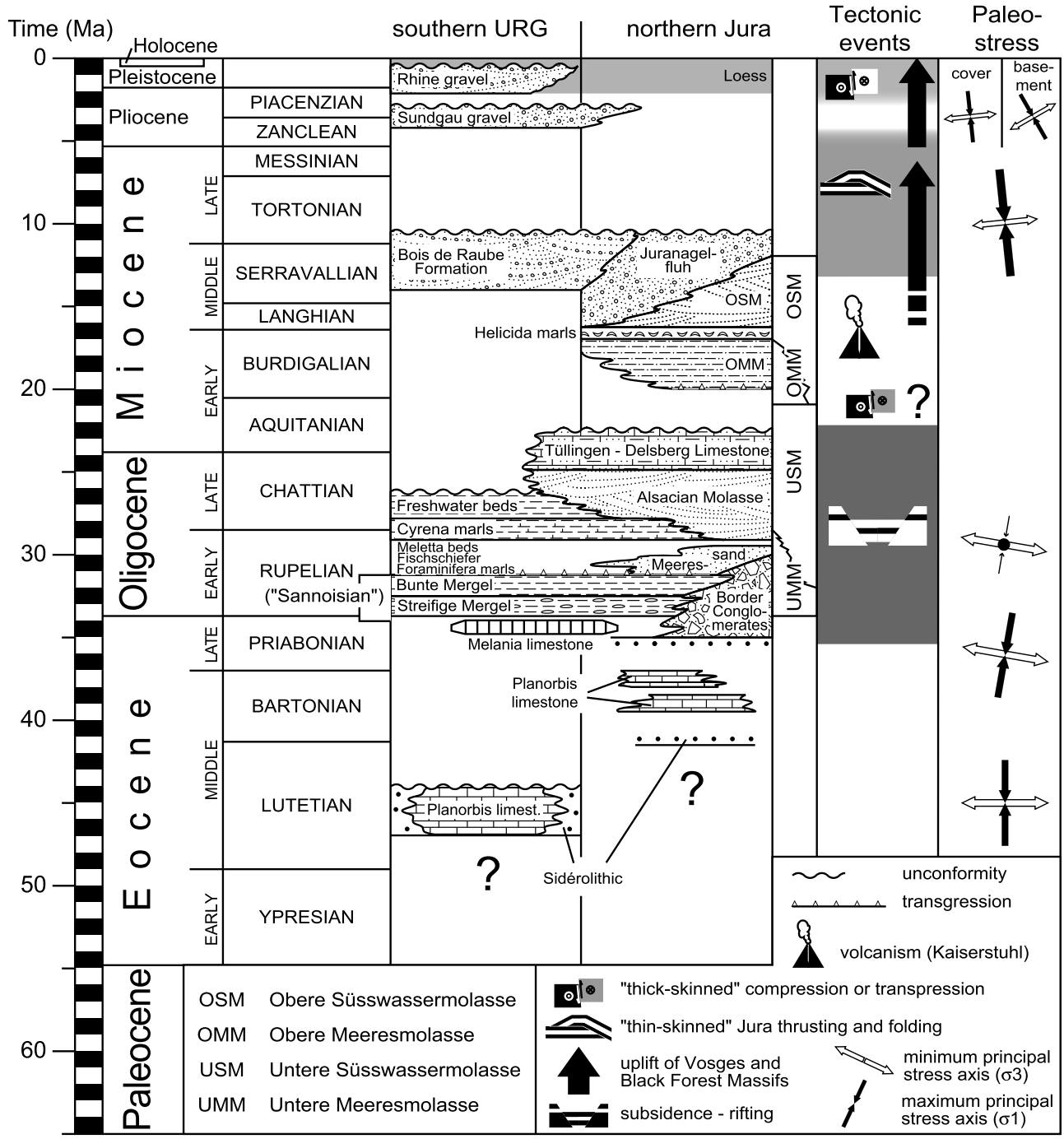

Figure 2. Chronostratigraphic chart showing the Cenozoic evolution of the southern URG and the southerly adjacent Jura, modified after *Giamboni et al.* [2004] (with kind permission of Springer Science and Business Media).

remained under the influence of NW-SE oriented compression. This led to erosion and/or nondeposition. Correspondingly, a major hiatus in the sedimentary record of the southern URG (Figure 2) largely prevents analysis of its evolution after the Earliest Miocene.

[4] A compressive reactivation of the URG border faults, such as the Rhine Graben flexure east of Basel, in the Burdigalian has been recently proposed [*Laubscher*, 2001, 2003]. However, exact age and causes of this flexuring remain unconstrained. Flexuring could equally well have been caused by the latest (earliest Miocene) stages of extension. The kinematics of early Miocene compressive events, which are linked to the widespread uplift of the Vosges–Black Forest arch, are yet only poorly constrained.

[5] Ongoing shortening in the Alps during the middle Miocene, leading to stacking of crustal slices in the external crystalline massifs of the Alps, and caused by ongoing subduction of European continental lithosphere [*Schmid et al.*, 1996], led to the decoupling of the Mesozoic sedimentary cover rocks along Mid to Late Triassic evaporitic series [*Burkhard and Sommaruga*, 1998]. This enabled the propagation of shortening across the Molasse Basin toward the foreland, incorporating the detached sediments into a deforming wedge and creating the folds and thrusts of the Jura Mountains (Figure 1). As a consequence, the Alpine thrust front propagated to the north and NW from the Serravallian (around 13 Ma) onward. The northernmost parts of the folded Jura, however, were probably not involved in deformation before early Tortonian times (see stratigraphic constraints given in Figure 2). The detached sediments were thrust onto the autochthonous cover of the foreland. In northern Switzerland, this autochthonous cover is frequently referred to as ''tabular Jura'' because of the horizontal layering of predominant Jurassic age sediments. At the junction to the URG, the detached sediments encountered preexisting structures inherited from Paleogene rifting, which had offset the Triassic décollement of the Jura Mountains. This inherited pattern influenced the shape of the northern parts of the developing thin-skinned fold-and-thrust belt [*Laubscher*, 1977, 1981; *Noack*, 1995]. The total shortening across the folded Jura, as measured between Molasse Basin and URG southwest of Basel, amounts to some 12 km [*Philippe et al.*, 1996].

[6] Since the late Pliocene (since about 3 Ma), NW-SE to N-S directed shortening has propagated northward and encroached on the southernmost parts of the URG [*Meyer et al.*, 1994; *Nivière and Winter*, 2000; *Giamboni et al.*, 2004]. While the foregoing deformation was largely restricted to the sediments detached along the Mid and Upper Triassic weak layers [*Philippe et al.*, 1996], this most recent shortening appears to be entirely rooted in the basement [*Meyer et al.*, 1994; *Giamboni et al.*, 2004]. In the present-day stress field the southeastern URG is subjected to sinistral transtensive strike-slip motion [*Larroque and Laurent*, 1988; *Schumacher*, 2002], as evidenced by the study of earthquake focal mechanisms [*Plenefisch and Bonjer*, 1997; *Deichmann et al.*, 2000; *Lopes Cardozo and Granet*, 2003; *Kastrup et al.*, 2004], whereas the area of the RBTZ is conceivably experiencing incipient dextrally transpressive inversion of Permo-Carboniferous troughs [*Meyer et al.*, 1994; *Ustaszewski et al.*, 2005b].

2. Analysis of Fault Slip Data and Paleostress Reconstruction

2.1. Fault Slip Data Collection

[7] The orientations of faults and corresponding striations (''fault slip sets'') were measured at numerous sites in the study area in order to derive the orientations of what is commonly referred to as the orientation of ''paleostress'' axes, although these axes often may reflect types of incremental or even finite strain rather than principal axes of the paleostress tensor. The majority of the data were acquired in Mesozoic limestones and to a lesser extent in Tertiary sediments (e.g., Figures 3a and 3c). Fault slip senses were inferred from various shear sense indicators on the fault planes [*Hancock*, 1985; *Petit*, 1987]. The most abundant indicators were slickolites (oblique stylolites), best developed in micritic Upper Jurassic limestones. Less frequently, slickenfibers (oblique fibrous growth) were found, mainly in oolithic limestones of both Mid and Upper Jurassic age (Figure 3b). Crescentic (or lunate) fractures, tensile cracks and/or Riedel shear planes were restricted to massive, coralliferous Upper Jurassic limestones and/or to cataclasites near to or directly within fault zones. Occasionally, pressure solution pits and striated pebbles (Figure 3a), horizontal stylolite peaks [*Plessmann*, 1972] or calcite-filled tension gashes (Figure 3c), were also used to infer the shortening directions.

[8] The quality of slip sense indicators was classified into ''excellent,'' ''good,'' and ''poor'' in order to allow for weighting during subsequent paleostress axes calculations. Additionally, the ''importance'' of faults was estimated in a qualitative manner based on (1) the dimensions of the exposed part of the fault plane, (2) the amount of displacement (if detectable), and (3) the presence or absence of cataclasite or fault gouge. Most of the analyzed faults, however, revealed slickolites associated with displacements in the order of a few millimeters only and thus record very small increments of strain.

[9] Overprinting relationships (crosscutting faults, superimposed slickensides, e.g., Figures 3a–3d) allowed establishing a relative chronology of faulting. This, in turn, permitted a separation of heterogeneous fault populations into homogeneous subsets that reflect one particular defor-

Figure 3. Selected examples of crosscutting relationships that constrain kinematics and relative age of deformation structures observed in the study area. (a) Shortening directions inferred from horizontal pressure solution pits and striations on limestone pebbles in lower Oligocene, grain supported conglomerates at the folded Jura front. Converging arrows indicate shortening direction. Pencil is for scale. (b) Superimposed slickensides on a steeply inclined fault plane in Oxfordian limestones. The older slickenside generation (L1) is related to Paleogene normal faulting. L2 forms both groove marks (gm) and fibrous steps (sf), which clearly overgrow L1. Coin for scale. (c) NNE trending joints in Chattian sands in the Delémont Basin. The joints, delineated by an oxidation front, are crosscut by en échelon aligned, calcite-filled tension gashes, suggesting that the joints accommodated minor sinistral strike-slip motion. (d) Equal-area projection of data from Figure 3c. (e) Southward tilted top-to-the-north thrust within Oxfordian limestones on the south limb of the Ferrette anticline. (f) Equal-area projection of fault slip data at Figure 3e, back rotated into a position where bedding is horizontal. All plots in this study are lower hemisphere, equal-area projections. See Figure 1 for locations of the outcrops.

mation phase only. The separation of polyphase fault populations was facilitated by the "incremental strain axes" or P-T axes method [*Marrett and Allmendinger*, 1990].

[10] Fault slip sets collected in tilted strata were rotated back into a position where bedding was horizontal before performing stress axes calculations. This procedure is justified by direct observations, which indicate that strata were mostly horizontal at the onset of reverse faulting/thrusting, yet before their involvement in folding (Figures 3e and 3f). The stress axes derived from back-rotated fault slip sets thus reflect the stresses at the onset of folding. Concerning the azimuths of the stress axes, the difference between "non-

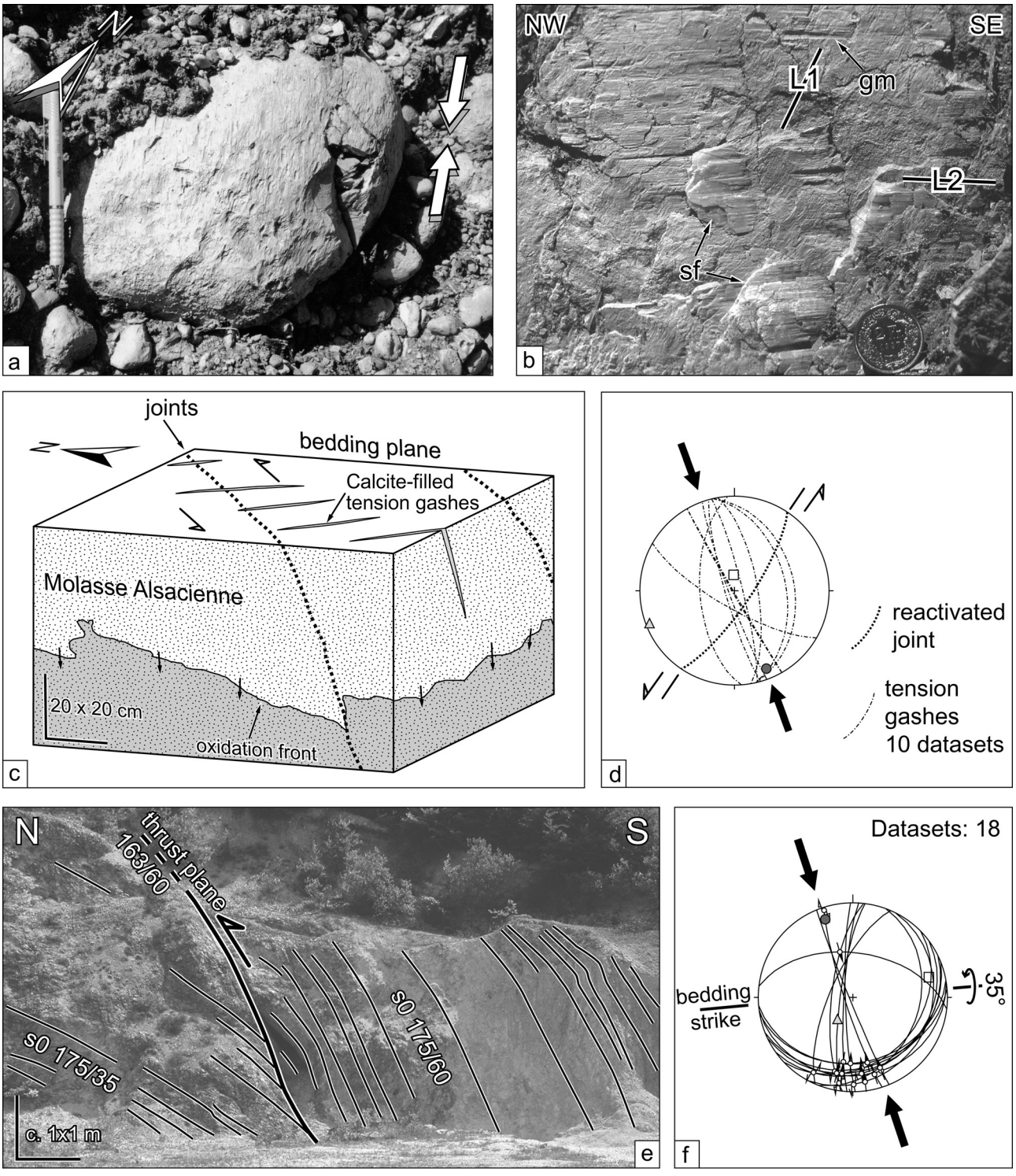

Figure 3

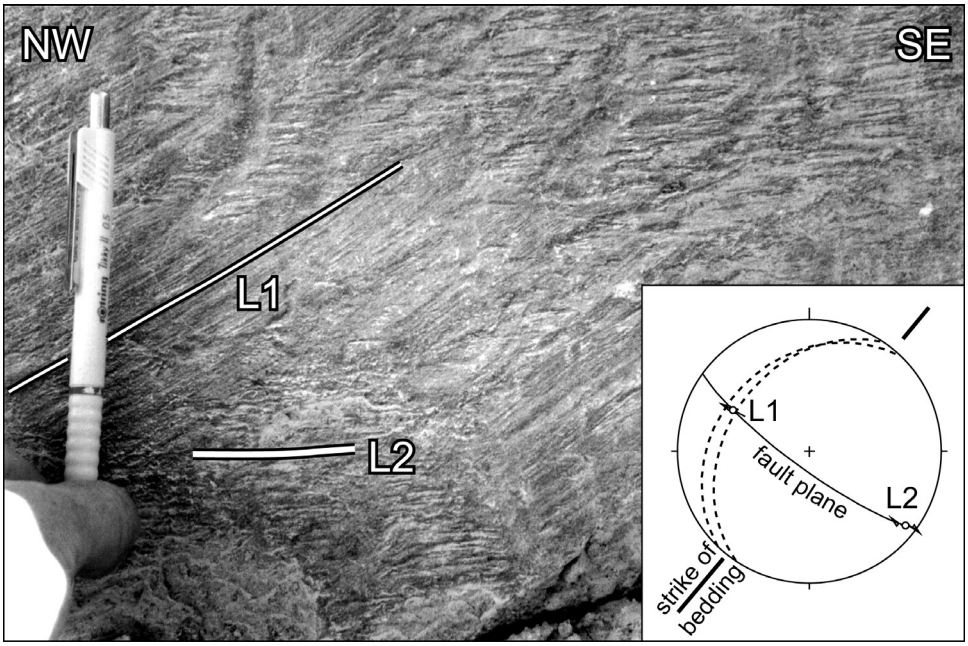

Figure 4. Repeated formation of horizontal slickensides on a fault plane in Mid-Jurassic limestones along the Jura front, concomitant with progressive tilting. New slickolites (L2) ''carve'' into older slickolites (L1) that were already tilted during an earlier folding increment. Inset is an equal-area projection of the data. See Figure 1 for location.

rotated'' and ''back-rotated'' fault slip sets was usually negligible, because few fault slip data were measured in strata inclined by more than some 40°.

[11] In this study, we focus on fault kinematics that postdate Paleogene rift-related extension of the URG recently described elsewhere [*Ustaszewski et al.*, 2005a]. Correspondingly, the fault kinematics described in the following represent already separated, homogeneous subsets of a more comprehensive analysis [*Ustaszewski*, 2004]. The structural data were visualized as lower hemisphere equal-area projections using computer program ''TectonicsFP,'' version 2.0 PR [*Reiter and Acs*, 1996–2000].

2.2. Crosscutting Relationships and Timing Constraints of Fault Kinematics

[12] Before presenting the results of the paleostress analysis it is necessary to address problems of repeated reactivation of preexisting faults, strain partitioning between strike slip faulting and folding, as well as relative and absolute timing constraints of the kinematics of faulting. In the following we present particularly clear examples that, amongst others, provide such valuable information.

[13] A particularly clear example for the repeated formation of horizontal slickolites along strike-slip faults and their subsequent tilting due to ongoing folding was observed in a locality along the NNE-SSW trending part of the Ferrette anticline (Fe in Figure 1) and presented in Figure 4. There, two generations of dextral slickolites on a subvertical fault plane, oriented perpendicularly to the strike of bedding, are observed. An older generation (L1) is overprinted by a younger generation (L2) that ''incises'' into L1. L1 is tilted by the same amount as the bedding planes, suggesting that it originally formed while bedding was still horizontal. After tilting of the beds due to folding during a second strain increment, pure dextral strike-slip faulting in a horizontal direction resumed, due to a third increment of deformation. This, and many other similar observations suggest that repeated permutation between folding and strike-slip faulting, such as postulated for the Jura arc in general [*Laubscher*, 1972], did also occur along the western rim of the Ferrette anticline.

[14] Exemplary observations pointing toward multiple reactivation of preexisting faults were also made near the northern tip of the Ferrette anticline, where the strike of this anticline abruptly sways around 60° from a NNE-SSW into an E-W trend. There (see data presented in Figure 5), NNE trending conjugate faults (inherited from Paleogene extension, Figure 5c) were first reactivated as extension veins that

Figure 5. Multiply reactivated faults in Mid-Jurassic limestones at the northernmost tip of the Ferrette Jura (fault slip set 31). Simultaneity of strike-slip faulting and folding accommodates extension perpendicular to the shortening directions. See Figure 1 for location. (a) and (b) Sinistral offset of preexisting extension veins, such as those plotted in Figure 5d, during Jura folding in late Miocene to early Pliocene times in a typical outcrop exhibiting fault reactivation. (c) Orientations of NNE trending conjugate faults inherited from Paleogene extension. (d) Orientations of extension veins accommodating E-W extension during (N)NE-(S)SW directed compression in the early Miocene(?). (e) Orientations of strike slip faults offsetting extension veins and formed during Jura folding in late Miocene to early Pliocene times.

accommodate E-W extension during (N)NE-(S)SW directed compression, presumably during the early Miocene (Figure 5d). The overall vein thickness amounts to approximately 15 meters in the outcrop. Later, i.e., during Jura folding in late Miocene to early Pliocene times the same veins became sinistrally offset (Figures 5a, 5b, and 5e). Horizontal slickensides reveal various pitch angles, often on the same fault plane. The latter observation again shows that

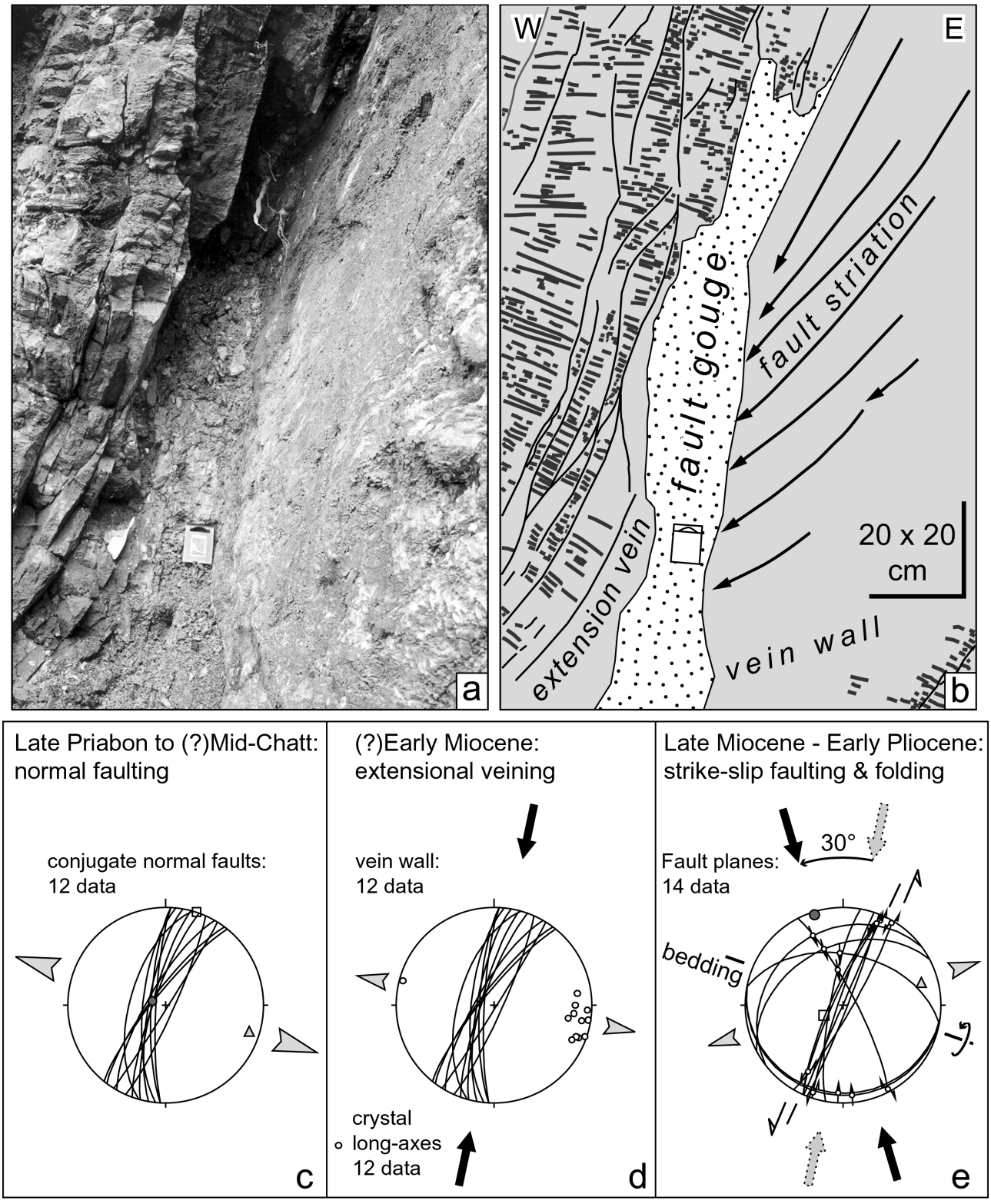

Figure 5

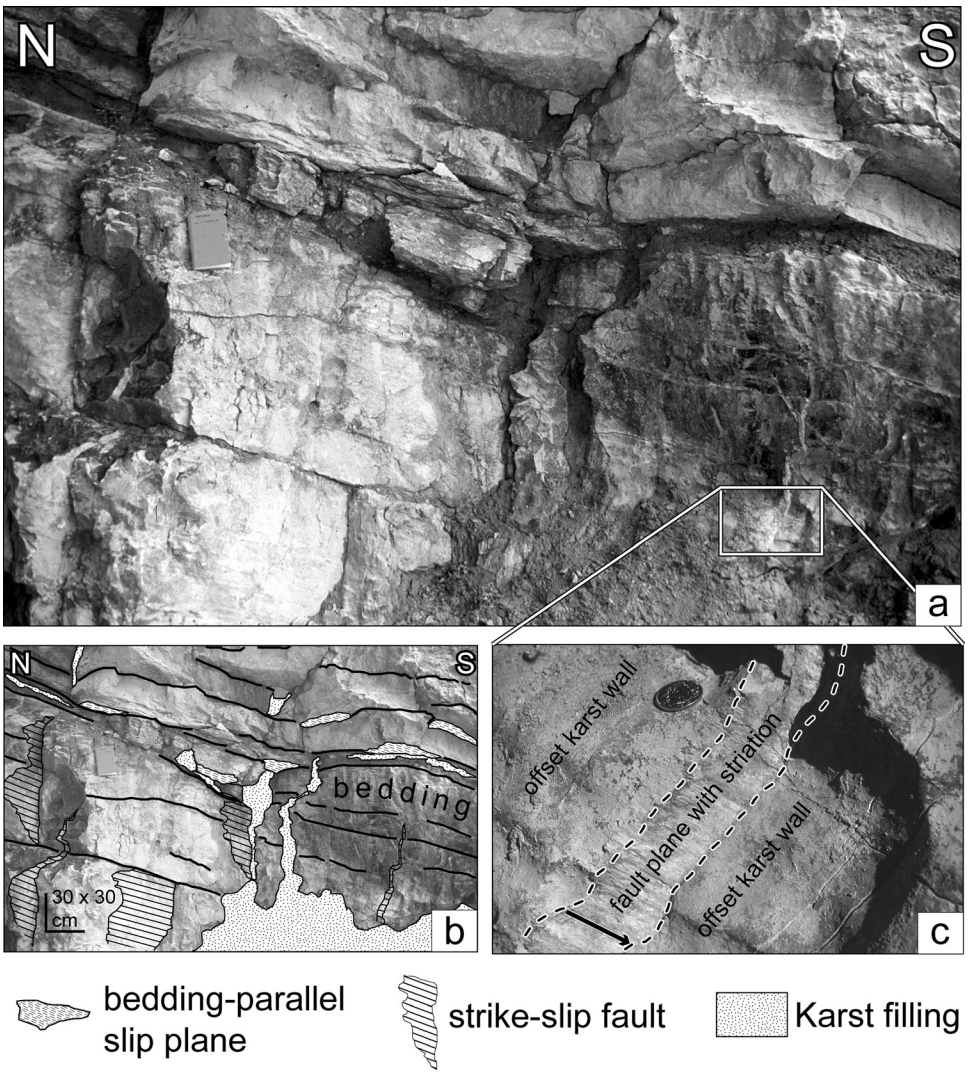

Figure 6. (a) Outcrop of Upper Jurassic limestones at the southern end of the Caquerelle anticline. The limestone is dissected by subvertical, NNE trending karst fissures that contain OMM-OSM sediments [*Hug et al.*, 1997a, 1997b]. The walls of the karst fissures are affected by sinistral strike-slip faults, which are partly offset themselves along bedding-parallel slip planes (evidenced by the fissure infill smeared out along bedding planes). (b) Interpreted line drawing of Figure 6a. (c) Detail of Figure 6a, coin for scale. See Figure 1 for location.

strike-slip faulting was concomitant with progressive folding at the Jura front. Since this intermittent strike slip faulting is linked to ENE-WSW extension, it indicates minor extension perpendicular to the dominant direction of horizontal shortening that is accommodated by folding/thrusting. This minor extension is probably linked to the formation of the tightly curved deformation front of the Ferrette anticline.

[15] At the southern end of the Caquerelle anticline (Ca in Figure 1) decimeter-bedded, Upper Jurassic limestones are dissected by NNE trending subvertical karst fissures, which most likely formed along Paleogene joints. The sedimentary infill of these fissures contains marine (at the bottom) and continental faunas (on top) of late Burdigalian to Serravalian age, which were correlated with deposits from the Molasse Basin south of the Jura Mountains [*Hug et al.*, 1997a, 1997b]. Small-scale sinistral strike-slip faults displace the karst fissures (Figure 6). However, the same fissures are also offset by bedding-parallel slip related to folding of the Caquerelle anticline, as can be judged from the sedimentary infill smeared out along bedding planes. These outcrop-scale observations not only provide excellent timing constraints but also show that the formation of Jura folds (such as the Caquerelle anticline) is intrinsically connected with the reactivation of preexisting, URG-parallel discontinuities. Such oblique folds form parallel to and above preexisting Paleogene normal faults that did offset the future décollement horizon. Figure 7 provides a schematic block diagram, further illustrating the sequence

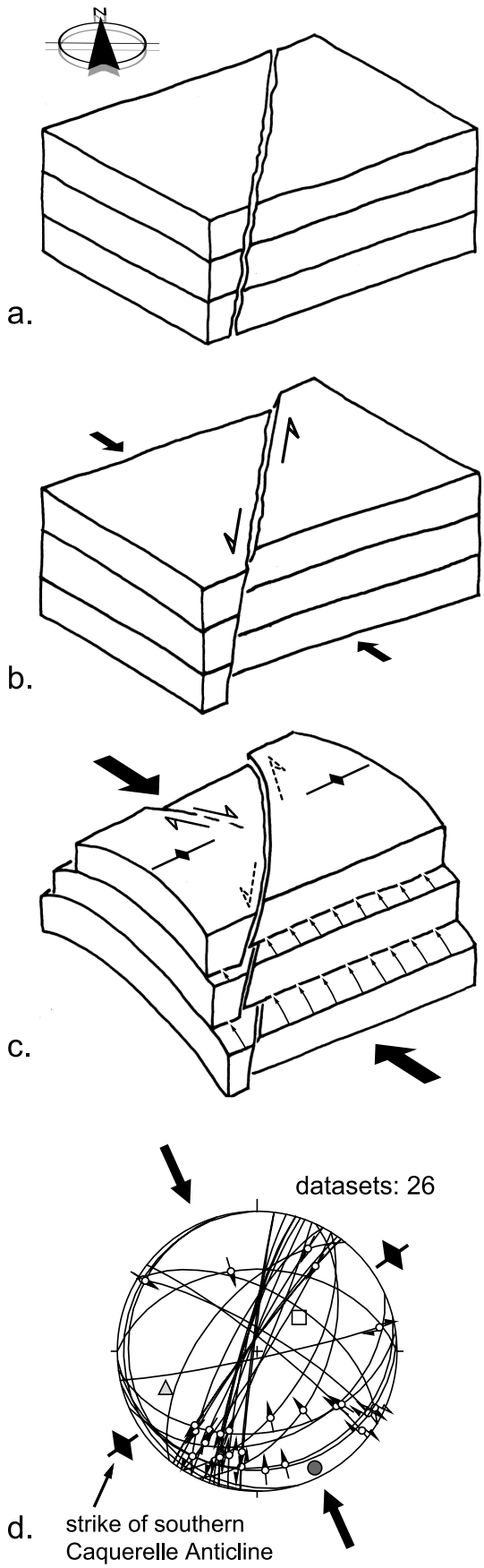

of deformation events recorded at the southern end of the Caquerelle anticline.

2.3. Paleostress Determination

[16] On the basis of superposition criteria such as those described above, more than 600 fault slip data collected at 60 localities were attributed to deformation that postdates Paleogene URG extension, linked to another set of fault slip data described elsewhere [*Ustaszewski et al.*, 2005a]. 53 fault-sampling localities yielded sufficient data for deriving the orientations of the principal kinematic axes and applying the inversion techniques described below. Each fault sampling location defined a data set consisting of a minimum of 2 and up to 41 fault slip sets.

[17] The orientations of the principal shortening, intermediate and extension axes have been primarily determined by applying the right dihedra method (RDM) [*Angelier and Mechler*, 1977; *Pfiffner and Burkhard*, 1987]. This method is a purely kinematic approach and applicable to any fault slip set. It only considers directions and senses of slip and makes no assumptions regarding the angle of internal friction. Strictly speaking, the RDM yields the finite strain axes of a population of fault slip sets [*Pfiffner and Burkhard*, 1987]. In order to conform to previous work, we refer to the axes derived with the RDM as "principal stress axes" ($\sigma1$, $\sigma2$ and $\sigma3$) or "paleostress" axes. The use of the RDM in the present study was justified because (1) the sampled fault slip sets usually showed a homogeneous spatial coverage, (2) only fault slip sets representing "pure shear" were considered for calculation (i.e., we rejected "simple shear" fault slip sets with one family of planes), and (3) the results were coherent with other "stress" markers observed, such as horizontal stylolite peaks. The results were considered reliable when the maxima and minima of the contours enclosed the positions of $\sigma1$ and $\sigma3$, respectively. This means that the obtained stress axes were kinematically consistent with the fault slip senses recorded. Fault slip data that were incompatible with the obtained stress axes were excluded from the data set, first eliminating faults exhibiting low-quality slip sense indicators. Furthermore, the results derived with the RDM needed to be coherent with results obtained with alternative methods applied to the same data set, namely the P-T axes method [*Marrett and Allmendinger*, 1990]. A drawback of the RDM is that the derived stress axis orientations do not necessarily reflect an "Andersonian" stress state with two horizontal and one vertical stress axes [*Anderson*, 1951], particularly when a data set consists of a blend of strike-

Figure 7. Schematic block diagram illustrating the deformation sequence as observed in Figure 6. (a) Bedded limestones dissected by NNE oriented karst fissures, which originated as Paleogene joints. (b) Sinistral reactivation of the karst fissures under compression. (c) Flexural-slip folding that partially offsets the fissures along bedding-parallel slip planes, but with strike-slip faulting continuing to a lesser extent. (d) Equal-area projection of data collected at the outcrop of Figure 6.

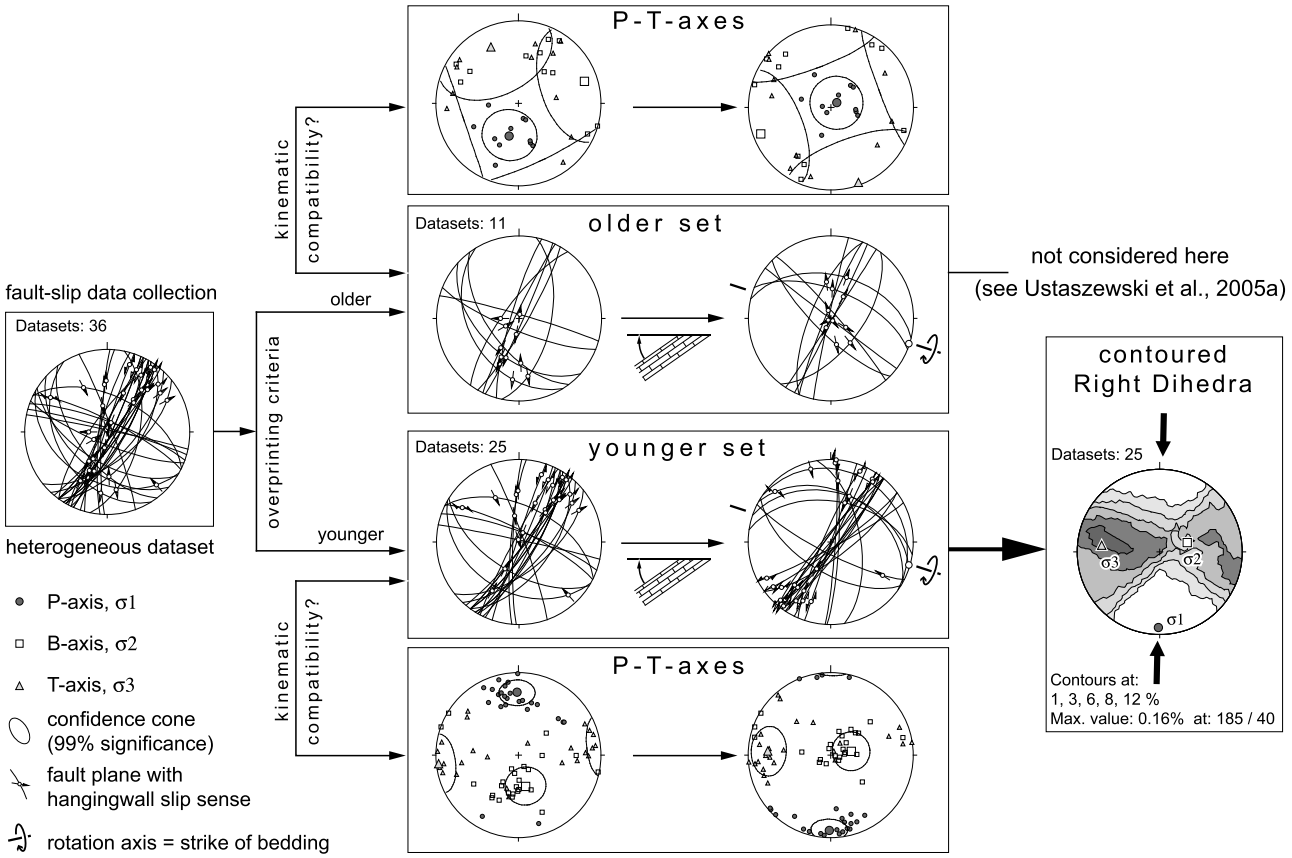

Figure 8. Flowchart illustrating the process of separating heterogeneous fault slip data into homogenous subsets by considering kinematic compatibility and overprinting criteria, as well as application of the right dihedra method to derive the paleostress axes.

slip and reverse faults. However, it was of predominant interest in this study to obtain the orientation of σ1, which proved to be subhorizontal for the majority of the data. The procedure of paleostress axes determination is exemplified for one fault slip set in Figure 8. In case of nonstriated faults or tension gashes, the "bisector method" [*Ustaszewski et al.*, 2005a] was applied for deriving the paleostress axes.

[18] The tectonic regime was inferred from the orientations of the principal stress axes and the distribution of P and T axes. Thereby we distinguished between (1) reverse faulting or thrusting (σ1 horizontal, σ3 vertical; well defined clusters of both P and T axes), (2) strike-slip faulting (σ1 horizontal, σ3 horizontal; well defined clusters of both P and T axes), (3) transpression (σ1 horizontal and well defined cluster of P axes, σ2 and σ3 poorly defined, great circle distribution of B and T axes), and (4) extension (σ1 vertical, σ3 horizontal). In case of small data sets (four or fewer data sets), no classification of the tectonic regime was made. The azimuths of σ1 and σ3 define what we will refer to as "shortening" and "extension" directions when analyzing these directions in map view. The principal stress axes determined at each site are summarized in Figure 9 and Table 1. The data sets are sorted from west to east. Shortening directions were plotted as converging arrows at the corresponding sites in Figure 10. Figure 10 also includes 11 data sets from the literature [*Philippe*, 1995; *Braillard*, 2006], as well as maximum horizontal stress directions inferred from in situ stress measurements in the sedimentary cover in order to compare the paleostress data with the recent stress field [*Reinecker et al.*, 2003].

[19] The orientations of the principal stress axes of the total of 53 data sets analyzed in this study are given in Figure 11. The salient feature of this compilation of new data is that azimuths of σ1 axes range from NW to NNE, clustering around a N-S orientation with a mean vector of 176/02. The σ3 axes, on the other hand, are distributed along an E-W oriented meridian, which reflects the tectonic regime characterized by the interchange between strike-slip and reverse faulting/thrusting. A nearly identical picture is obtained when only the data sets from the folded Jura are considered (Figure 11, bottom). In map view (Figure 10), the shortening directions reveal a slightly northward diverging fan shape. This divergence is particularly pronounced at the immediate Jura front. In the west and along NNE trending anticlines shortening directions are generally (N)NW oriented. Toward east, they tend to sway into a north to NNE orientation.

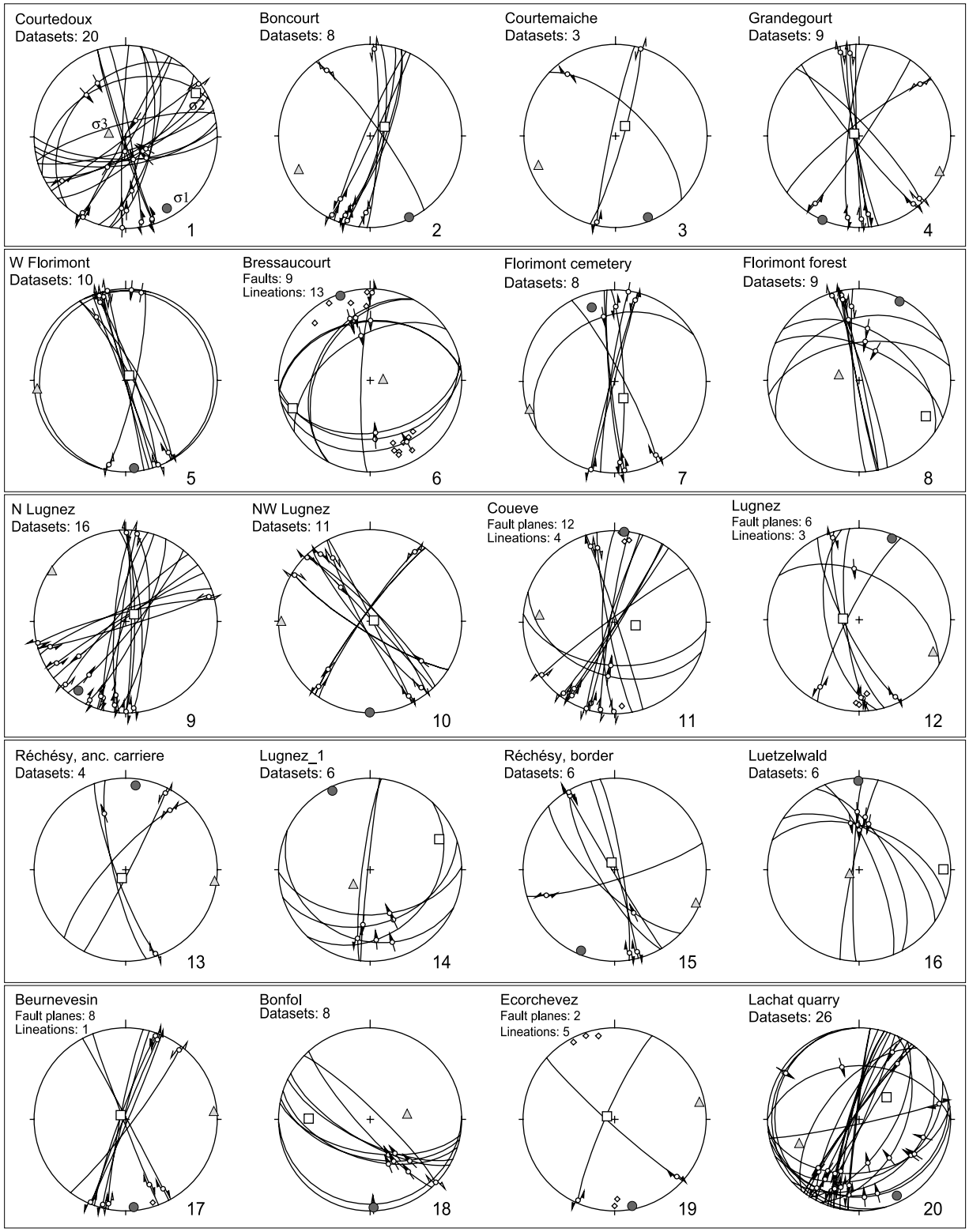

Figure 9. Equal-area projections of fault sets and paleostress axes orientations obtained at 53 sites. Numbers at the lower right of each plot correspond to the numbering of the data sets in Table 1.

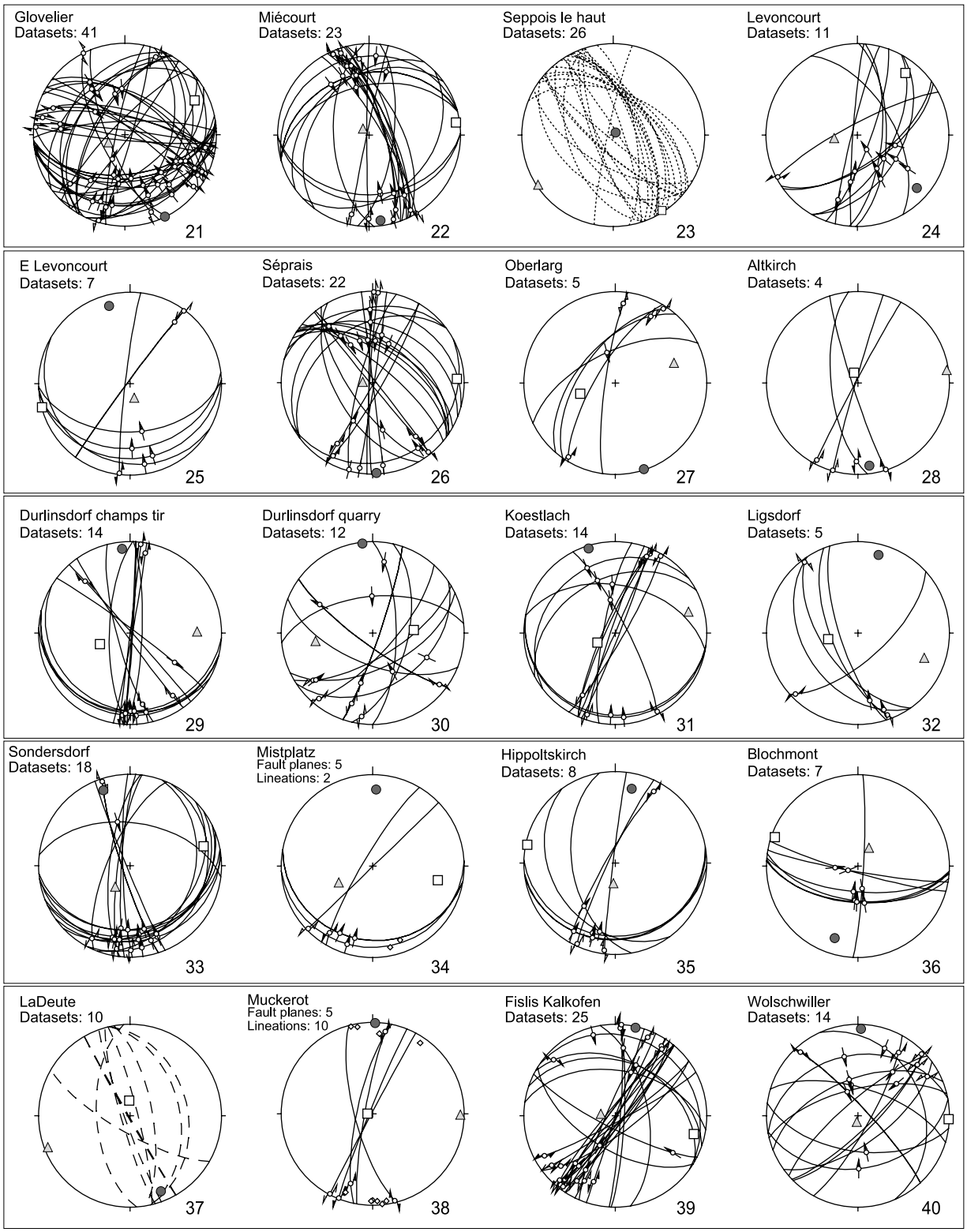

Figure 9. (continued)

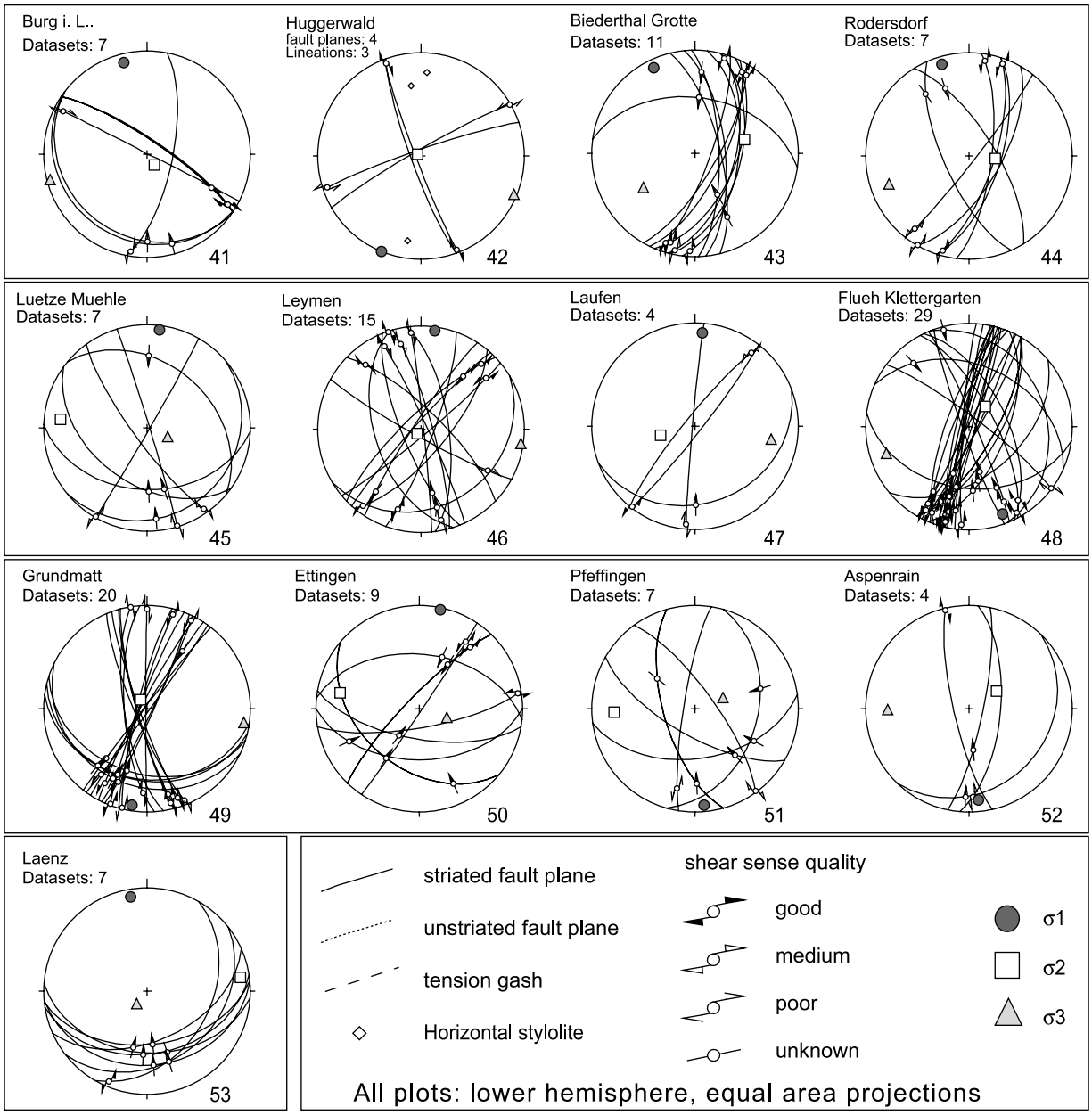

Figure 9. (continued)

[20] Three domains that comprise areas where the anticlines strike NNE, i.e., parallel to preexisting normal faults related to the opening of the URG, were defined (see domains 1, 2, and 3 in Figure 10). Domain 1 encompasses the entire Caquerelle anticline. Domains 2 and 3 compose the west segment of the Ferrette and Landskron anticlines, respectively. The large number of individual fault slip sets collected in these domains was combined into the data sets for these domains as presented in Figure 12. Figure 12 (left) shows bulk paleostress axes and contoured dihedra for these domains. In all three domains, the shortening directions are consistently NNW oriented. In domains 1 and 2, the contours indicate that the orientations of $\sigma 1$ axes are well defined, while $\sigma 3$ directions define a girdle. This again indicates a transpressive regime in which strike-slip faulting and folding/thrusting interchanged. The contours for domain 3, however, reveal well-defined maxima for both $\sigma 1$ and $\sigma 3$, indicating a strike-slip regime for this domain. An important feature common to all three domains is the obliquity between fold trend and shortening directions (Figure 12, right). The shortening directions are at angles between 40° and 48° with respect to the NNE trending anticlines. Note that several fault slip sets measured within the three domains represent bedding-parallel slip planes that are directly related to folding. This, together with the observed obliquity between fold trend and shortening di-

Table 1. Paleostress Reconstruction Sites With Prevalent Lithology and Stratigraphic Age[a]

Site	Location	X	Y	Age	s1_azi	s1_pln	s2_azi	s2_pln	s3_azi	s3_pln	N	n	Regime
1	SW Courtedoux (JU)	567800	249175	Kimmeridge	150	11	058	11	284	75	20	1	transpression
2	Boncourt JU	568400	260500	Oxford	154	02	058	75	245	15	8	0	strike-slip
3	west Courtemaiche JU	569750	256640	Oxford	158	05	044	78	249	11	3	0	strike-slip
4	Grandegourt JU	570650	257940	Oxford	204	01	294	85	114	05	9	0	strike-slip
5	west Florimont	571000	261950	Oxford	180	07	034	82	270	05	10	2	strike-slip
6	SE Courtedoux JU	571275	250350	U Priabon to L Rupel	342	03	252	15	074	75	9	0	reverse
7	Florimont village	572100	262175	Oxford	343	17	153	73	252	03	8	1	strike-slip
8	Florimont forest	572425	261900	Oxford	027	03	118	18	287	71	9	1	strike-slip
9	south Courcelles	573250	260000	Oxford	214	09	050	80	305	03	16	0	strike-slip
10	NW Lugnez JU	573400	259775	Oxford	180	01	079	86	270	04	11	0	strike-slip
11	Coueve JU	574075	256725	Oxford	006	01	098	71	276	19	12	0	strike-slip
12	Lugnez JU	574560	258975	Kimmeridge	022	05	273	76	113	13	6	0	strike-slip
13	SW Rechesy	574790	261050	Oxford	007	08	204	82	097	02	4	0	unknown
14	north Lugnez JU	574925	260150	Oxford	334	05	066	19	230	71	6	0	reverse
15	SE Rechesy	576325	261050	Oxford, U Priabon to L Rupel	202	05	338	83	112	05	6	0	strike-slip
16	east Rechesy	577075	261450	Oxford	359	03	090	09	250	81	6	0	reverse
17	Beurnevesin JU	577275	260300	L Kimmeridge	175	04	311	84	085	04	8	0	strike-slip
18	north Bonfol JU	577650	259250	L Kimmeridge	178	04	271	33	081	56	8	0	reverse
19	SE Vendlincourt JU	578775	255275	Oxford	169	04	291	83	078	06	2	0	strike-slip
20	west Glovelier JU	580300	242100	Upper Oxford	154	08	051	58	248	30	26	0	transpression
21	Glovelier JU	580660	241990	Kimmeridge	154	00	064	16	245	74	41	0	transpression
22	NW Miécourt JU	580700	253575	Kimmeridge	172	07	082	05	316	82	23	2	transpression
23	Seppois-le-Haut	581600	264400	Pliocene	037	87	146	01	236	03	26	0	extension
24	east Levoncourt	583075	255700	Oxford	132	14	038	15	262	69	11	0	transpression
25	east Levoncourt	583375	255850	Bajoc-Bathon	345	13	255	00	163	77	7	1	transpression
26	Séprais JU	584200	246700	Kimmeridge	178	01	087	09	275	81	22	3	transpression
27	north Oberlarg	584800	256950	Oxford	162	01	253	57	071	33	5	1	strike-slip
28	Altkirch	585500	275800	lower Rupel	172	08	304	81	080	05	4	0	strike-slip
29	Durlinsdorf	585625	259550	Bajoc-Bathon	355	08	250	61	089	27	14	2	transpression
30	Durlinsdorf	585900	259450	Bajoc-Bathon	353	02	086	53	262	37	12	1	transpression
31	Koestlach	588100	261600	Bajoc-Bathon	343	03	242	72	074	18	13	0	transpression
32	west Ligsdorf	589225	257750	Oxford	015	13	258	63	110	23	5	0	strike-slip
33	west Sondersdorf	591400	259275	Oxford	341	14	075	18	216	67	18	3	reverse
34	SW Luppach	591500	261075	Oxford	003	17	102	28	244	56	5	0	reverse
35	Hippoltskirch	592775	258075	Oxford	012	18	282	02	186	72	8	0	reverse
36	SSW Blochmont	592875	255160	Oxford	198	19	289	04	031	71	7	1	reverse
37	south Delémont JU	593150	244320	Chattien	158	13	359	76	249	05	10	0	strike-slip
38	Muckerot	594812	259525	Oxford	001	01	278	86	091	04	5	0	strike-slip
39	south Fislis	594879	260800	Oxford	013	01	103	13	277	77	25	1	transpression
40	south Wolschwiller	597300	255950	Oxford	002	06	092	01	191	84	14	0	reverse
41	Burg im Leymental BL	600000	256200	Oxford	346	09	146	80	255	03	7	0	reverse
42	Huggerwald SO	600200	252750	Oxford	202	00	295	87	112	03	4	0	unknown
43	Biederthal	600500	257100	Oxford	334	09	074	49	237	40	11	0	transpression
44	Rodersdorf SO	601675	258600	Oxford	343	08	095	69	251	19	7	1	strike-slip
45	Muehle Luetzeltal	601700	252750	Oxford	007	05	276	17	112	72	7	0	unknown
46	Leymen	603300	259850	Oxford	008	04	222	85	098	03	15	0	strike-slip
47	Muehle Laufental	604000	251325	Oxford	005	10	255	62	100	26	4	0	unknown
48	east Flüh SO	605150	258750	Oxford	159	10	039	70	252	17	29	0	transpression
49	Grundmatt, south Ettingen BL	607225	258300	Oxford	189	06	324	81	098	06	20	0	transpression
50	south Ettingen BL	607525	258350	Oxford	012	02	281	23	107	67	9	0	reverse
51	Pfeffingen BL	610075	256800	Oxford	175	07	268	23	068	66	7	1	unknown
52	Chollholz BL	617825	262375	Bajoc-Bathon	172	16	055	56	271	27	4	0	unknown
53	south Diegten BL	627325	249800	Torton	350	08	082	09	219	77	7	1	reverse

[a]Swiss National coordinates are used; s1_azi, s2_azi, s3_azi are azimuth of sigma1, −2 and −3, respectively; s1_pln, s2_pln, s3_pln are plunge of sigma1, −2 and −3, respectively; N is number of fault slip sets per site; and n is number of faults with unknown slip sense. JU, BL, and SO are abbreviations for the Swiss cantons of Jura, Basel Landschaft, and Solothurn, respectively; U and L are abbreviations for upper and lower, respectively.

rection, suggests that the folds formed as ramp anticlines above sinistral oblique ramps.

2.4. Calculation of "Stress Ratios" for Two Areas Characterized by Oblique Ramps Associated With Jura Folding

[21] It is very likely, and in many cases even proven, that fault slip data, such as those that yielded the kinematically compatible paleostress orientations presented above, were generated by the reactivation of preexisting faults or other preexisting discontinuities that slipped by frictional sliding. Hence inferring stress ratios from three-dimensional unscaled Mohr diagrams, such as those presented in Figure 13 obtained from paleostress data collected within domains 1 and 2 outlined in Figure 10, i.e., from domains encompassing sinistral oblique ramps, yields valuable in-

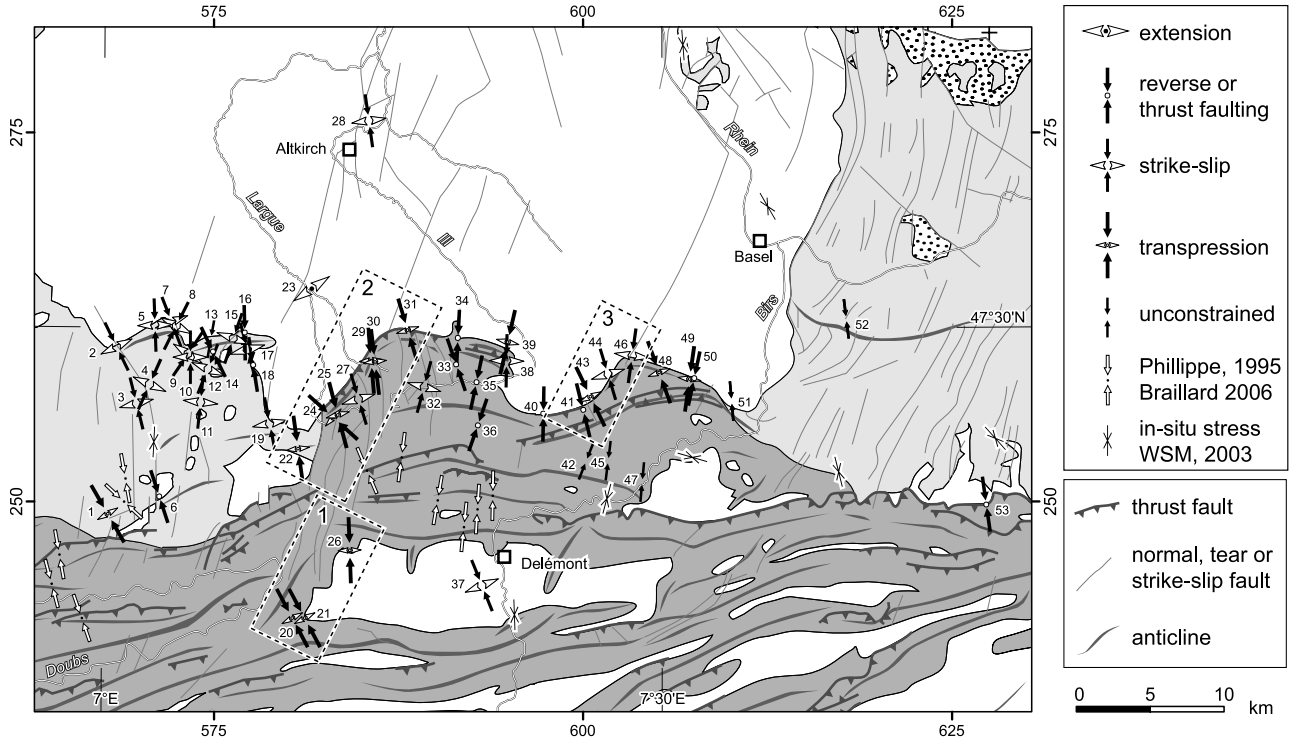

Figure 10. Shortening (converging arrows) and extension directions (diverging arrows) derived for the northernmost Jura and adjacent URG [*Philippe*, 1995; *Braillard*, 2006]. In situ stresses in the sedimentary cover, taken from the World Stress Map Project (WSM) [*Reinecker et al.*, 2003], are plotted for comparison. Numbers at map edges are Swiss National coordinates in kilometers. Patterns are identical to those used in Figure 1. Numbering of the data sets corresponds to Table 1 and Figure 9. Dashed rectangles numbered 1 to 3 depict the domains considered in Figure 12.

formation regarding the type of bulk strain achieved by the activation of a large number of fault slip sets.

[22] The reduced unscaled three-dimensional "stress tensors" for the fault slip data presented in Figure 13 were determined by the numerical dynamic analysis [*Sperner and Ratschbacher*, 1994], after first determining the finite strain axes orientations for the bulk data sets with the RDM, i.e., after first finding the best kinematic solution. An angle of 45° was chosen between the incremental shortening axis P and the individual fault striation. In doing so, the "stress axes" determined by the NDA coincide with those determined by the purely kinematic approach of the RDM. For each tensor we also calculated the average misfit angle α, which is the deviation between the calculated slip lineation and the measured lineation for each fault slip pair. The angle α allows evaluating the quality of the computed stress tensors. In addition, the tensor quality rank TQR (TQR = $n(n/N)/\alpha$) is indicated [*Delvaux et al.*, 1997], which is another mean to assess the quality of the calculated stress tensors. TQR values greater than 1.5, such as obtained in our case, are considered very reliable (Figure 13 and Table 1).

[23] As is seen from inspection of the data compiled in Figure 13, the R ratio is very small, implying that the "stress difference" $\sigma2-\sigma3$ is very much smaller compared to the stress differences $\sigma1-\sigma2$ or $\sigma1-\sigma3$. In terms of stress, these data would imply a frequent exchange between $\sigma2$ and $\sigma3$ during progressive deformation, hence a change between thrust and strike-slip mode while the subhorizontal $\sigma1$ direction remains constantly N-S oriented, such as postulated for Jura folding on a large scale [*Laubscher*, 1972]. However, we prefer to look at these data in terms of the finite strain, which is produced by the partitioning between strains achieved by fault slip sets that accommodate thrusting and strike slip deformations, respectively. According to our interpretation in terms of finite strain, in combination with the information provided by Figure 12, we infer from Figure 13 that the amount of strain achieved by strike slip faulting nearly equals that achieved by thrusting. This results in an oblate strain ellipsoid and points to the nearly equally important role of strike slip faulting along preexisting NNE-SSW oriented faults, inherited from Paleogene rifting, as compared to thrusting and/or folding related to the formation of the transverse Ferrette and Caquerelle folds. Hence, in the case of these anticlines extreme caution has to be taken when inferring amounts of shortening and/or applying models regarding the formation of arcuate mountain belts [*Hindle and Burkhard*, 1999] from two-dimensional cross sections only, as has recently been discussed by *Affolter and Gratier* [2004].

2.5. Stratigraphic Constraints Regarding the Timing of Deformation Related to the Analyzed Fault Slip Data

[24] Constraints on the timing of deformation have recently been improved and this section compares these new

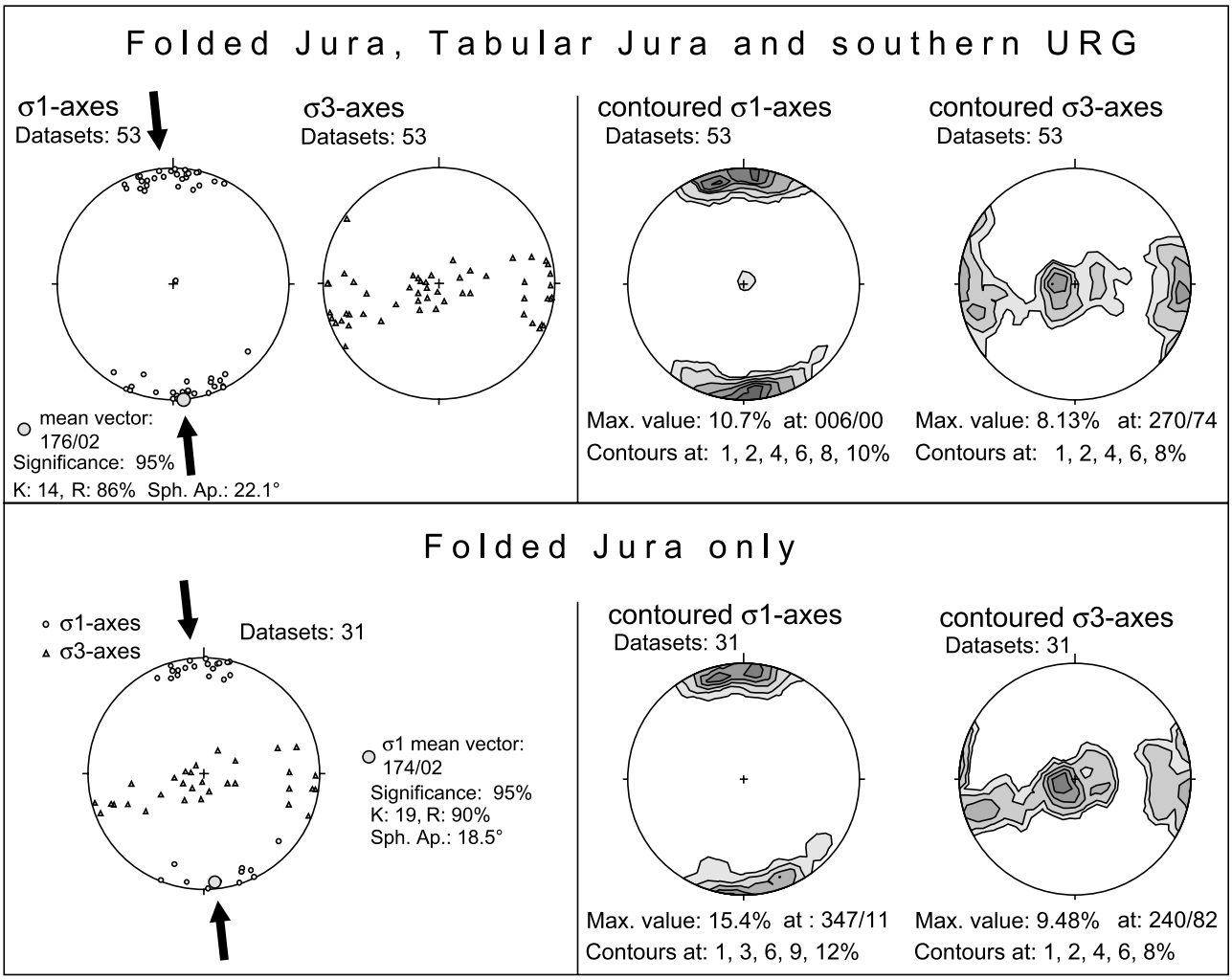

Figure 11. Paleostress axes from 53 sites collected in this study. (top) Data comprising the URG and the folded and tabular Jura. (bottom) Data sets collected in the folded Jura only.

data with previously reported data. The maximum age of faulting associated with the formation of the northernmost part of the Jura fold-and-thrust belt is late Serravallian to Tortonian, as given by the youngest sediments affected by deformation. This constraint is provided by the Serravalian to Tortonian "Bois de Raube" and "Juranagelfluh" gravels (Figure 2), which were shed from the Vosges and Black Forest massifs, respectively [*Kälin*, 1997; *Kemna and Becker-Haumann*, 2003]. The Bois de Raube gravels crop out in the Ajoie and in the western Delémont basins, and they are separated from the Vosges by the Vorbourg and Caquerelle anticlines (Figure 1). The "Juranagelfluh" gravels are found in the eastern Delémont Basin, in the Laufen Basin and in the tabular Jura SE of Basel (Figure 1). Mammal remains in the Bois de Raube Fm. provided an age between 13.8 and 13.2 Ma for the southern occurrences (Delémont Basin) and a slightly younger age of 10.5 Ma for the northern occurrences (Charmoille Basin, CB in Figure 1) of these deposits [*Kälin*, 1997]. These data provide a maximum age for folding of the Vorbourg (Vb in Figure 1) and Caquerelle anticlines of around 13 Ma, while thrusting of the frontal Jura fold-and-thrust belt onto the autochthonous foreland did not occur before about 10.5 Ma [*Becker*, 2000].

[25] The timing brackets regarding the minimum age of the Jura fold-and-thrust belt are less numerous and conclusive. In the southern folded Jura near Neuchâtel the horizontally layered infill of karstic fissures found in an inclined limb of an anticline NW of Neuchâtel yielded a mammalian fauna with ages that range between 4.2 and 3.4 Ma [*Bolliger et al.*, 1993; *Steininger et al.*, 1996]. Hence, at this locality folding had ended before these fissures were filled in. However, this timing bracket does not necessarily constrain the minimum age of the detachment of the Jura fold-and-thrust belt at its northern edge (i.e., within our study area), since deformation probably migrated in sequence toward the foreland.

[26] Clear evidence for later deformations is now available for the area of the autochthonous Mesozoic cover north of the Jura fold-and-thrust belt (northern part of our study area in the Ajoie, see Figure 1). The Sundgau area (Figure 1) is nestled by the fluvial "Sundgau gravels," which were

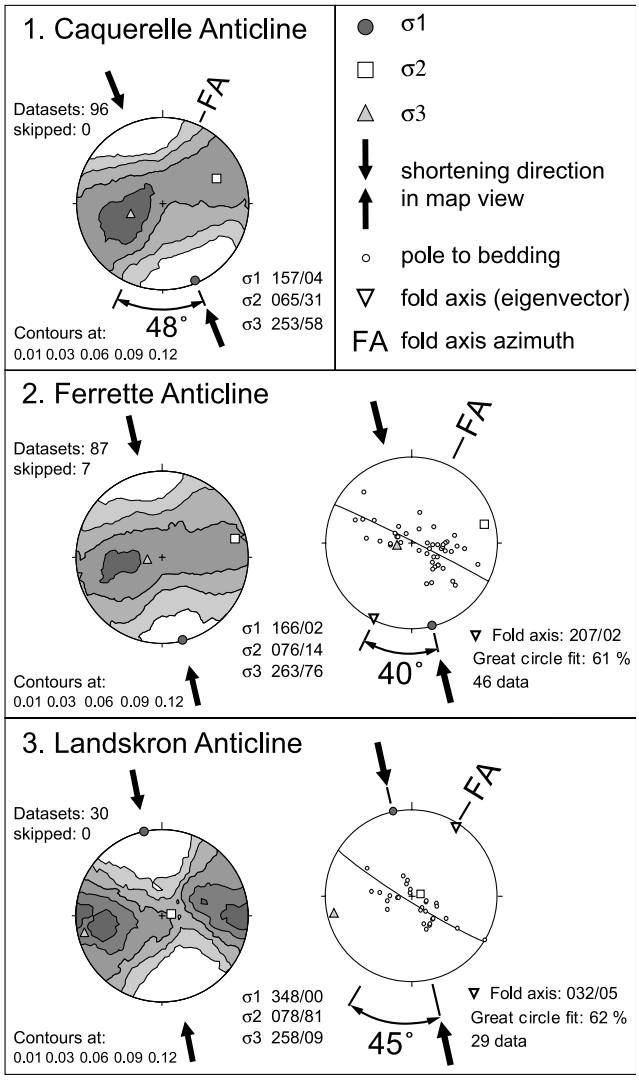

Figure 12. Contoured dihedra and paleostress axes derived in three domains in the folded Jura (see Figure 10 for location), demonstrating obliquity between shortening directions and fold trends. The trends of the fold axes (right) are taken from tectonic maps (domain 1) or calculated from dip data (domains 2 and 3) by eigenvector analysis.

deposited in an alluvial plain by an anostomosing braided river system and which were subsequently gently folded [*Giamboni et al.*, 2004], thus providing evidence for late Pliocene to recent deformations in this area. The stratigraphic age of the gravels, determined by mammal stratigraphy, ranges between 4.2 and 2.9 Ma [*Petit et al.*, 1996].

[27] Although gently folded [*Giamboni et al.*, 2004] and locally faulted (such as at locality 23 listed in Table 1 [see also *Ustaszewski et al.*, 2005b]), we interpret the deposition of the Sundgau gravels as postdating the formation of the thin-skinned Jura fold-and-thrust belt, based on all data and observations available so far. The current extent of the Sundgau gravels is clearly limited to an area in the northern part of the tabular Jura of the Ajoie area and the southern part of the URG, where they are found immediately adjacent to the front of the Ferrette anticline (Figure 1). However, no such gravels are found above the Ferrette anticline [*Giamboni et al.*, 2004] or above the detached Mesozoic of the Jura fold-and-thrust belt in general. This suggests that the gravels were never deposited in the area of the detached Mesozoic in the first place, or alternatively, that they were eroded later on and concomitant with the formation of the Ferrette anticline. We give clear preference to the first hypothesis according to which a topographic swell, provided by the front of the detached Mesozoic, i.e., the preexisting Ferrette anticline, would have prevented deposition of the Sundgau gravels in the area of the detached Mesozoic, indicating that the Ferrette anticline already existed as a topographic feature. Hence the formation of the classical thin-skinned Jura fold-and-thrust belt in general probably predates the onset of deposition of these gravels at 4.2 Ma. This would be in perfect agreement with the constraints available for the more internal parts of the folded Jura discussed above. The alternative hypothesis

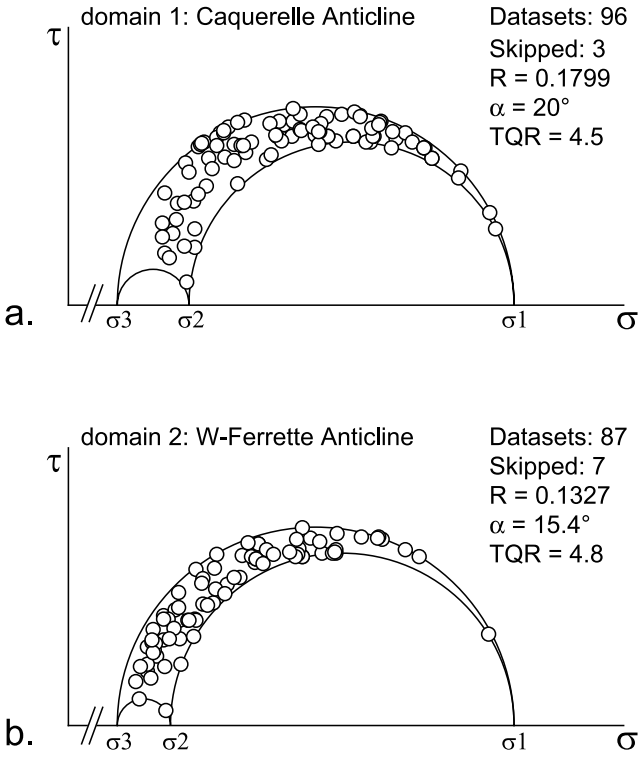

Figure 13. Mohr circle diagrams for estimating stress ratios from fault slip sets along oblique ramps in the domains of the (a) Caquerelle and (b) Ferrette anticlines (outlined in Figure 10). Mohr circles were calculated for a reduced stress tensor that corresponds to the kinematic solution of the RDM. Parameters are α, average misfit angle; TQR, tensor quality rank [*Delvaux et al.*, 1997]; TQR, $n(n/N)/\alpha$, where N is number of data per site and n is number of data with known slip sense. See text for further discussion.

is rejected because we would expect that Pleistocene deposits found along the northern slopes of the Ferrette anticline, constituting its erosional veneer, contain a large amount of Alpine-derived material typical of the Sundgau gravels [*Théobald et al.*, 1958; *Liniger*, 1970; *Ruhland et al.*, 1973] together with the locally derived material of Jurassic age. This is clearly not the case as the slope deposits along the Ferrette anticline contain exclusively locally derived Jurassic material and definitely no eroded and redeposited Sundgau gravels [*Schneegans et al.*, 1934]. In summary, it is concluded that the biostratigraphic age of the Sundgau gravels [*Petit et al.*, 1996] provides a lower time bracket for thin-skinned Jura folding and thrusting that ended about 4.2 Ma.

[28] The fault sets we collected within the detached Mesozoic include striated pebbles and small-scale reverse faults observed within the ''Juranagelfluh'' Formation, found beneath and in front of the frontal Jura thrust, where the Triassic décollement emerges to the surface (data set 53 in Figures 9 and 10 and Table 1). Consequently, the fault slip sets collected in the folded Jura domain and presented in this work are considered to have probably formed between about 13 Ma (10.5 Ma in the north) and about 4.2 Ma.

[29] In the autochthonous Mesozoic and the area of the URG (Figure 1) it is not easy to decide as to when the measured fault sets formed, since this area is clearly also affected by post-4.2 Ma thick-skinned deformation [*Giamboni et al.*, 2004; *Ustaszewski et al.*, 2005b], suggesting further northward propagation of shortening. Only in one case could data have been obtained within the very poorly outcropping Sundgau gravels (locality 23 in Figure 9). It is likely that the fault slip data found in the immediate foreland of the frontal Jura thrust can be attributed to horizontal far-field stresses exerted by the nascent thin-skinned Jura belt onto its autochthonous foreland before about 4.2 Ma. On the other hand, the paleostress data obtained on fault sets formed during the formation of the two en échelon-aligned anticlines at the tabular Jura–URG boundary (F and R in Figure 1), can be attributed to post-late Pliocene shortening, coeval with the folding of the Sundgau gravels [*Giamboni et al.*, 2004]. These data do not show significant deviations from those obtained further to the south (Figures 10 and 11). Note also that the maximum horizontal stress directions derived from in situ stress measurements are largely identical with those derived from the paleostress analysis within both the folded and tabular Jura (Figure 10). It is therefore concluded that no major change of the stress field did occur after about 4.2 Ma, i.e., after the onset of thick-skinned deformation of the autochthonous Mesozoic and the Tertiary deposits of the URG north of the thin-skinned Jura fold-and-thrust belt.

3. Inferences From Map View and Newly Constructed Cross Sections

[30] The Ferrette and Landskron anticlines, i.e., the northernmost anticlines of the folded Jura depicted in Figure 14, abruptly change strike by some 60–70°. The western, NNE trending segments of the two anticlines are oriented parallel to a pair of prominent west dipping Paleogene normal faults of the URG, both of them delimiting half grabens. The geometry of these half grabens can be inferred from the Base-Tertiary surface contours shown in Figure 14, constructed from reflection seismic lines and well data [*Ustaszewski*, 2004].

[31] Two boreholes, whose locations are indicated in Figure 14, provide evidence that Mesozoic sediments of the northern limb of the Ferrette anticline overthrust Paleogene synrift deposits of the URG, as depicted in Figure 15a. The NNE trending part of the Ferrette anticline exposes Lower to Mid-Jurassic sediments in its core. The entire western part of the Ferrette Jura is dissected by a dense array of tear faults that trend at angles of 15–20° to the strike of the anticline. Several anticlines appear sinistrally dragged along these NNE oriented faults.

[32] At the northernmost tip, where the anticline abruptly sways into an ESE orientation, a minor top-to-the-south backthrust delimits a transpressive pop-up (see profile in Figure 15b). Toward the ESE, the amplitude of the Ferrette anticline progressively diminishes until the gently folded Mesozoic strata plunge beneath Paleogene synrift sediments of the Tertiary fill of the Allschwil half graben, located between the Ferrette and Landskron anticlines (Figure 14). The associated axial plunge of the Ferrette anticline toward east is again a feature inherited from rifting, since the prerift Mesozoic sediments originally, i.e., before the formation of the Ferrette fold, gently dipped toward the east within the Allschwil half graben.

[33] The four cross sections across the Ferrette Jura depicted in Figure 15 roughly trend parallel to the shortening directions derived from the fault slip data analysis. At the same time they are not everywhere perpendicular to the macrostructures they traverse. Particularly cross sections 1–1′ is oriented obliquely to the structural grain (Figure 14). Cross sections 1–1′ and 2–2′ (Figures 15a and 15b) were constructed using existing geological maps [*Schneegans et al.*, 1934; *Diebold et al.*, 1963; *Liniger*, 1970; *Ruhland et al.*, 1973; *Dannecker*, 1995], well logs [*Schneegans and Théobald*, 1948] and structural data collected by *Dannecker* [1995] and in the course of this study. Cross sections 3–3′ and 4–4′ (Figures 15c and 15d) have been modified after *Ruhland et al.* [1973] and *Fischer* [1965], respectively. Cross section 5–5′ (Figure 16) is part of a migrated reflection seismic profile shot by Enterprise Oil in 1987.

[34] As is obvious from inspection of Figure 14, the western, NNE trending segment of the Ferrette anticline is located above an oblique ramp that nucleated above the steeply west dipping, Paleogene Ferrette normal fault bounding the Ferrette half graben. This graben-bounding normal fault was overthrust by the advancing Jura front, as is evidenced by boreholes [*Schneegans and Théobald*, 1948]. Furthermore, several sinistral strike-slip faults, along which out-of-plane movements occurred, traverse those two cross sections.

[35] Cross section 2–2′ (Figures 14 and 15b) traverses the Ferrette anticline at the point where its strike changes from a NNE trend into an ESE orientation. This position marks the transition from the sinistral oblique ramp to a frontal ramp. This cross section also traverses the western

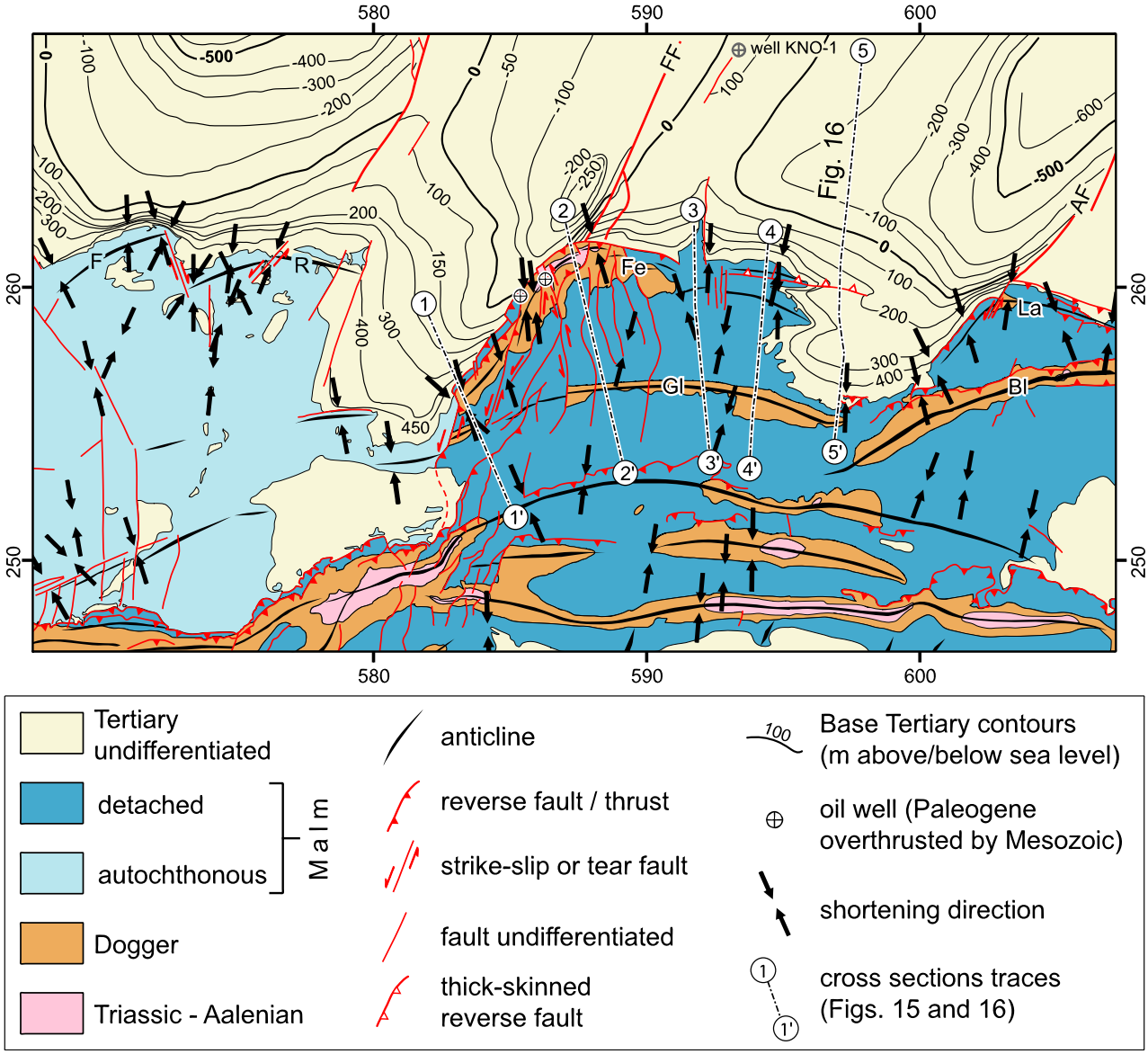

Figure 14. Geologic tectonic map of the northernmost folded Jura. The frontal Ferrette and Landskron anticlines change their trend by some 60–70° along strike. Their western segments are parallel to (and partly overthrust) Paleogene half grabens. The shortening directions (converging arrows) tend to sway from a (N)NW into a north to NNE orientation along strike from west to east. Labeling of anticlines and faults corresponds to Figure 1. Numbers at map edges are Swiss National coordinates in kilometers.

end of an anticline located south of the Ferrette fold: the Glaserberg anticline (Gl in Figure 14). Note that the north limb of this gentle anticline is considerably steeper than its south limb and that the flat-lying Mesozoic strata north of this anticline are found at a relatively lower elevation north of this anticline. This suggests that the Glaserberg anticline nucleated above a preexisting E-W striking basement step that was associated with extensional flexuring of the Mesozoic strata. Such east to ENE trending extensional flexures of Paleogene age are typical of the southern end of the URG [*Ustaszewski et al.*, 2005a]. They were studied in detail at the northern edge of the tabular Jura in the Ajoie (the Florimont and Réchésy anticlines indicated in Figures 1 and 14). Their en échelon alignment has resulted from sinistral transtensive strike-slip faulting during the Paleogene along preexisting Late Paleozoic ENE trending basement faults underlying the flexures [*Ustaszewski et al.*, 2005a, 2005b]. Note that the Glaserberg and Blauen anticlines, as well as two minor flexures in the autochthonous Mesozoic immediately west of the Glaserberg anticline, are also aligned en échelon (Figures 1 and 14). These en échelon flexures originally formed as Paleogene extensional flexures related to sinistral transtension above basement faults. In the case of the Glaserberg and Blauen anticlines these preexisting flexures controlled the nucleation of anticlines during the décollement of the detached Mesozoic

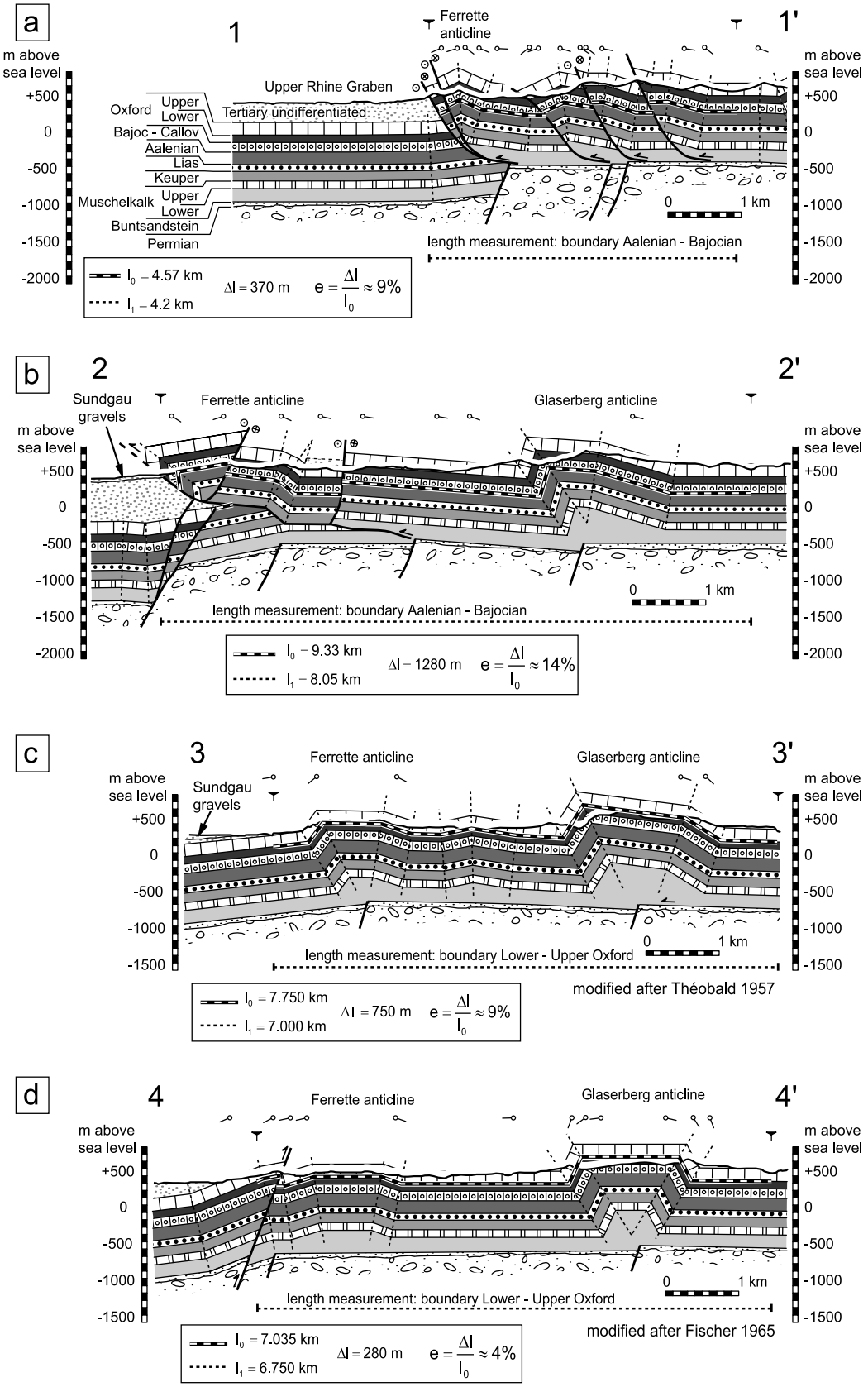

Figure 15. Cross sections across the Ferrette Jura constructed roughly parallel to the shortening directions derived in this study (Figures 9 and 10). See Figure 14 for location of the sections.

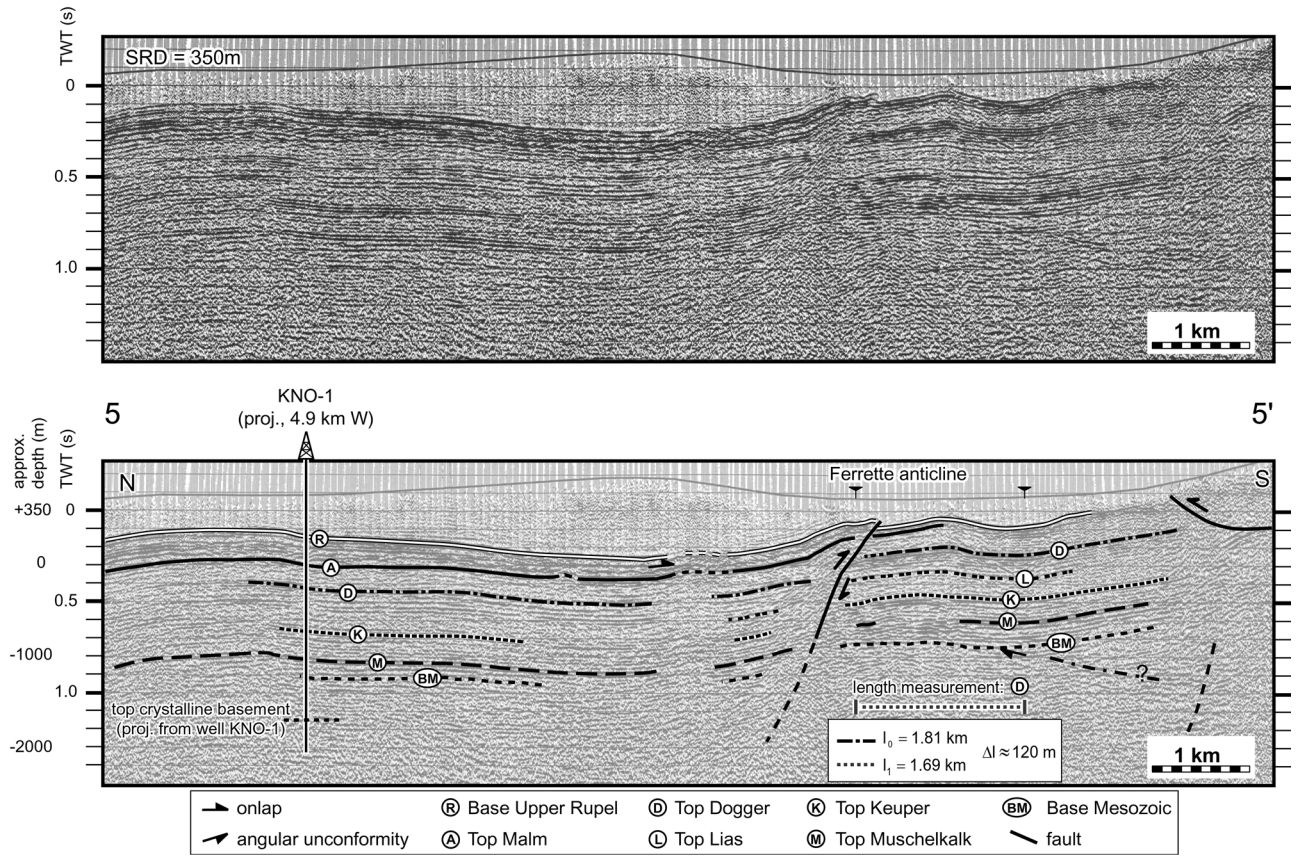

Figure 16. N-S trending industry-type reflection seismic line traversing a compressively reactivated Paleogene extensional flexure. For location see Figure 14. Seismic data are the courtesy of Enterprise Oil.

cover (Figure 15) before about 4.2 Ma, while in the case of the very gentle Florimont and Réchésy folds the associated discrete basement steps were compressively reactivated in late Pliocene to recent times [*Giamboni et al.*, 2004; *Ustaszewski et al.*, 2005b]. Transpressive deformation along the western, NNE trending part of the Ferrette anticline, well documented by the fault slip data (Figures 10 and 12), implies that movements must also have occurred in and out of the plane of cross sections 1–1′ and 2–2′ (Figures 15a and 15b). Hence the shortening e ($e = dl/l_0$, $dl = l_0 - l_1$), estimated for all five cross sections by comparing deformed (l_1) and restored lengths (l_0) of marker horizons does not take into account horizontal shortening caused by out-of-plane strike-slip displacements and hence underestimates the amount of shortening in a direction parallel to these two sections. Bed lengths were measured between the northernmost occurrences of Mesozoic sediments and the horizontally layered sediments south of the Glaserberg anticline (see pin points given in Figure 15). In cross section 5–5′ (seismic section of Figure 16), the vertical scale roughly equals the horizontal scale within the Mesozoic sediments. It was thus admissible to compare the deformed and restored length of the well visible "D" reflector at a depth of ~0.2 s two-way traveltime in the southern part of the section. Shortening in section 1–1′ is in the order of 9%. Cross section 2–2′ reveals a shortening of 14%, before decreasing to 9% and 4% in sections 3–3′ and 4–4′, respectively. Hence the greatest amount of within-plane shortening is achieved along section 2–2′. The component of shortening related to the formation of the Glaserberg anticline essentially remains constant in sections 2–2′ to 4–4′. Hence the differences in the amount of total in-plane shortening regarding sections 2–2′ to 4–4′ are entirely due to the changing geometry of the frontal Ferrette anticline. The westward increasing amount of shortening also finds its expression in map view, in that the oldest outcropping sediments in the Ferrette anticline (Aalenian shales) crop out only in the west (Figure 14). Note also that the gentle Ferrette anticline in the east laterally transforms into a frontal thrust some 2.5 km east of the northernmost tip of the Ferrette Jura (see Figures 15b–15d).

[36] At the northern edge of section 4–4′, where shortening accommodated by the Ferrette anticline is very minor (Figure 15d) and where the Mesozoic strata defining this gentle fold dip beneath the synrift sediments of the Paleogene Allschwil graben (Figure 14), a steeply north dipping, top-to-the-south reverse fault truncates the north limb of the anticline. The reflection seismic line situated further east (cross section 5–5′ of Figure 16) shows the continuation of this structure beneath the Paleogene synrift fill of the URG. The seismic cross section reveals an extensional flexure in

the Mesozoic strata, on lapped by synrift sediments of Paleogene age, as inferred from the southward tapering wedge (between the reflectors marked A and R in Figure 16). The flexure sits above an E-W trending, north dipping high-angle basement fault of late Paleozoic origin and reactivated a first time during Paleogene rifting [*Ustaszewski et al.*, 2005a]. However, this same basement fault was reactivated a second time in compression, as is inferred from the steeply north dipping, top-to-the-south reverse fault that truncated the synrift fill and that almost reaches to the surface. Since this fault clearly cuts through the décollement horizon, it most probably formed during the thick-skinned post-4.2 Ma stage. Similar features were observed elsewhere [*Giamboni et al.*, 2004; *Ustaszewski et al.*, 2005b]. It is important to note that the position of this top-to-the-south reverse fault coincides with an anticline detected by the folding of the base of the Sundgau gravels [*Giamboni et al.*, 2004; *Ustaszewski et al.*, 2005b], which proves its post-late Pliocene age and its most probably thick-skinned origin. This observation confirms that pre-4.2 Ma Jura décollement tectonics were followed by thick-skinned tectonics.

[37] When calculating the amount of within-plane shortening along profiles $4-4'$ and $5-5'$ depicted in Figure 15 we subtracted the shortening due to this thick-skinned stage. This allows discussing the diverging shortening directions observed in the area of the Ferrette and Landskron anticlines, and possibly associated rotations, during the thin-skinned stage of Jura folding, as is presented below.

4. Discussion

4.1. Why Do Shortening Directions Fan Toward North at the Jura Front?

[38] The shortening directions in the study area, obtained from paleostress analysis of fault slip data above, are consistently NNW to NNE oriented. In general, this confirms earlier studies on a larger scale [*Plessmann*, 1972; *Meier*, 1984; *Philippe*, 1995]. Our study, however, reveals a gentle fanning of the shortening directions toward north, particularly at the frontal Ferrette and Landskron anticlines. Moreover, several NNE-SSW trending, transpressional anticline segments, such as the western parts of the Ferrette and Landskron, as well as the entire Caquerelle anticline (Figure 10), show a pronounced obliquity between the structural grain and the shortening directions (Figures 12 and 13). This clearly suggests their origin as ramp anticlines above sinistral oblique ramps. In addition, the shortening in the frontal Ferrette anticline increases along strike from east to west (Figures 15 and 16). However, transpressional deformation across the NNE trending, oblique ramp segment of this anticline implies that within-plane shortening deduced from cross sections of any orientation underestimates the total shortening. In the following, we further analyze the northward fanning of shortening directions in conjunction with the observed westward increase of shortening across the frontal Ferrette anticline in order to discuss the role of possible block rotations around vertical axes during décollement.

[39] First, we attempt to estimate the strike-slip component along the oblique ramp. To overcome the lack of suitable markers, we assume that the total shortening in the oblique ramp segment of the Ferrette anticline (in an N-S direction) can be partitioned into a component perpendicular to the oblique ramp and a strike-slip component parallel to it. Figure 17a shows the shortening amounts derived from the cross sections as black arrows plotted onto the trailing (= southern) ends of the cross section traces. The arrows lengths are drawn to scale. An E-W trending reference line was drawn south of the Ferrette anticline. Next, the shortening amounts in the sections with no out-of-sections movements ($3-3'$ to $5-5'$) were plotted at the intersections of this reference line with the traces of the corresponding cross sections (gray arrows in Figure 17a). The leading edges of these arrows define a WNW-ESE trending line. The intersection between this line and the E-W trending reference line defines a point of zero N-S shortening, situated east of cross section $5-5'$ (open circle in Figure 17a). Assuming that the shortening increased linearly toward west, the two diverging lines were extrapolated westward until they intersected with the trace of the NNE trending basement fault (the nucleus of the oblique ramp). This yields the total shortening of 1.4 km at the northern tip of the Ferrette anticline (arrow labeled c in Figure 17a). The strike-slip component along the oblique ramp (dashed black line in Figure 17a) can now be deduced from

$$b = c \cos\alpha.$$

[40] For $\alpha = 25°$, this yields $b = 1.27$ km (Figure 17a, top left inset). The westward increase of shortening across the Ferrette anticline necessitates a clockwise rotation of the detached sediments of $\sim 6.5°$ around a vertical axis, located at the pole of no shortening (open circle in Figure 17a). Paleomagnetically determined clockwise rotations of $\sim 10°$ SE of the Ferrette Jura [*Gehring et al.*, 1991] confirm this assumption (Figure 17b), further implying that the detached sediments have undergone rotations on a still larger scale between inherited NNE trending oblique ramps. The northward fanning of shortening directions in map view therefore reflects the transition from pure N-S convergence in the eastern, E-W trending part of the Ferrette anticline to sinistral transpression along the NNE oriented oblique ramp segment (schematic strain ellipses in Figure 17b). The fan shape of shortening directions was possibly emphasized by a passive clockwise rotation of the ''less shortened'' east part of the anticline during detachment, at a time when shortening along the oblique ramp segment may still have been active. This scenario is supported by paleomagnetic evidence.

[41] In summary, we propose the scenario for the formation of the frontal Jura anticlines sketched in Figure 17c. As the deformation front advanced toward the foreland, the detached sediments encountered a NNE trending, Paleogene basement fault that was obliquely oriented to the displacement direction (large white arrow in Figure 17c) and which had offset the basal Triassic décollement. The deformation front east of the NNE trending fault was successively

transferred to the north along a sinistral oblique ramp that formed above this discontinuity. This led to sinistrally dragged anticline crests (Figures 14, 17b, and 17c). Shortening concentrated at the transpressional oblique ramp and decreased toward east. This along-strike decrease of shortening induced a clockwise rotation of the detached sediments, which passively rotated the less shortened, east part of the anticline, producing northward fanning shortening directions. These considerations on the kinematics of the Ferrette Jura front are summarized in a schematic block diagram (Figure 18). They appear to be also applicable to the Landskron anticline, given the great similarities among these two frontal folds.

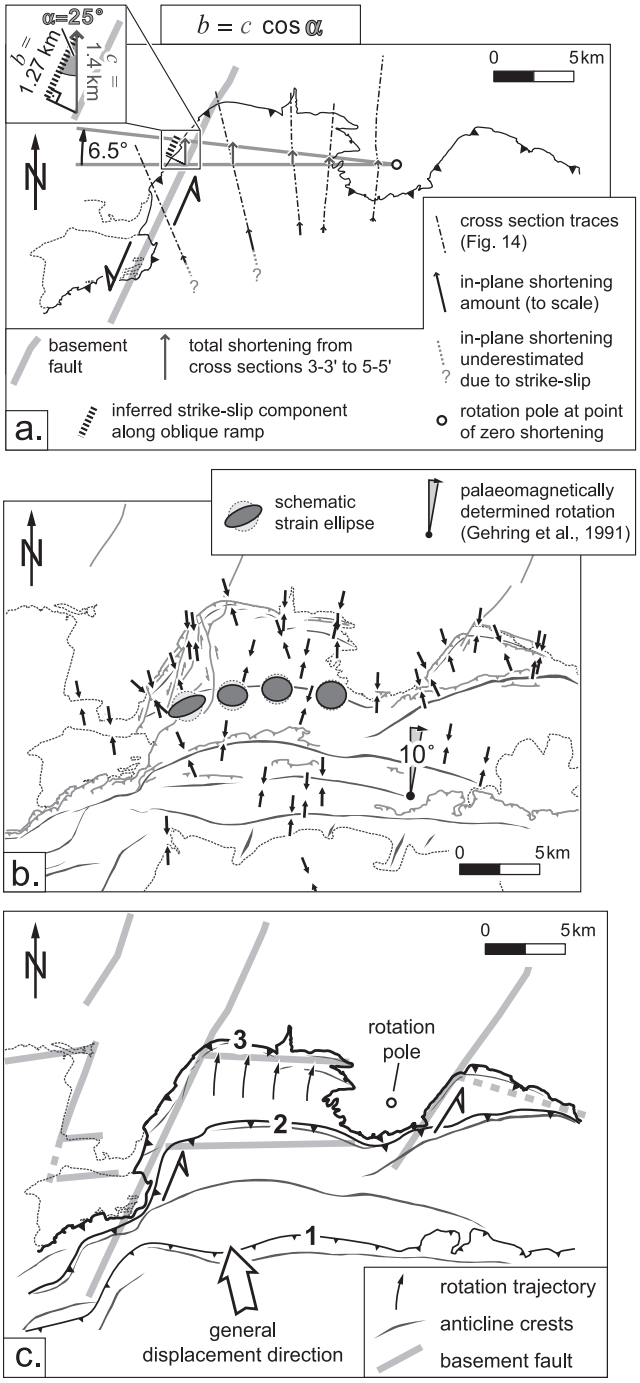

4.2. What Induced the Change From Thin-Skinned to Thick-Skinned Deformation During the Late Pliocene?

[42] We regard the evidence for basement-rooted fault reactivation to have followed late Miocene to early Pliocene thin-skinned folding and thrusting as conclusive [see also *Giamboni et al.*, 2004; *Ustaszewski et al.*, 2005b]. However, it appears surprising at first sight that this transition occurred without any (detectable) reorientation of the maximum horizontal stresses in the sedimentary cover. The thick-skinned reactivation is particularly well documented in an ENE trending belt of basement faults that delineate the Permo-Carboniferous graben system in the subsurface, roughly paralleling the northern front of the eastern Jura Mountains [see *Ustaszewski et al.*, 2005a, Figure 2]. Our data suggest that this transition is linked to the incipient inversion of these grabens, which implies that shortening within the pre-Mesozoic basement, taking place within the Alps during classical Jura folding ("Fernschub" or "distant push" theory in the sense of *Laubscher* [1961]) migrated northward into the Alpine foreland during the late Pliocene. On the basis of evidence from reflection seismic profiles and cross section balancing considerations, inversion of Permo-Carboniferous grabens underneath the western Jura belt during a late stage or, alternatively, postdating thin-skinned Jura folding and thrusting, was already invoked earlier [*Philippe*, 1994; *Philippe et al.*, 1996]. More recently, geomorphologic evidence from the southernmost URG revealed the spatial coincidence between gentle anticlines in the base of the Pliocene fluvial Sundgau gravels and transpressively/compressively reactivated basement faults [*Giamboni et al.*, 2004; *Ustaszewski et al.*, 2005b].

[43] In the following, we speculate on the reasons that might have led to the transition from thin-skinned tectonics to basement-rooted deformation. Two possibilities are briefly outlined: (1) deactivation of intracrystalline glide along the

Figure 17. Kinematic considerations on the northward fanning of shortening directions along the Ferrette Jura. (a) Estimation of the strike-slip component along the oblique ramp segment of the Ferrette anticline. Extrapolation of the N-S shortening obtained from cross sections (Figures 15 and 16) toward west gives the total shortening at the northern tip of the anticline. The strike-slip component is then deduced from disassembling the total shortening into a component parallel to the oblique ramp. (b) Schematic strain ellipses across the Ferrette Jura, superimposed onto surface fault pattern, anticline crests and shortening directions from Figure 14. The paleomagnetically determined clockwise rotation is in agreement with the rotation implied by the model in Figure 17a. (c) Successive northward advance of the deformation front due sinistral transfer along NNE trending normal faults and concomitant rotation of the detached sediments, shown at three stages. Numbers indicate 1, Vorbourg anticline; 2, Glaserberg–Blauen anticlines; 3, Ferrette–Landskron anticlines.

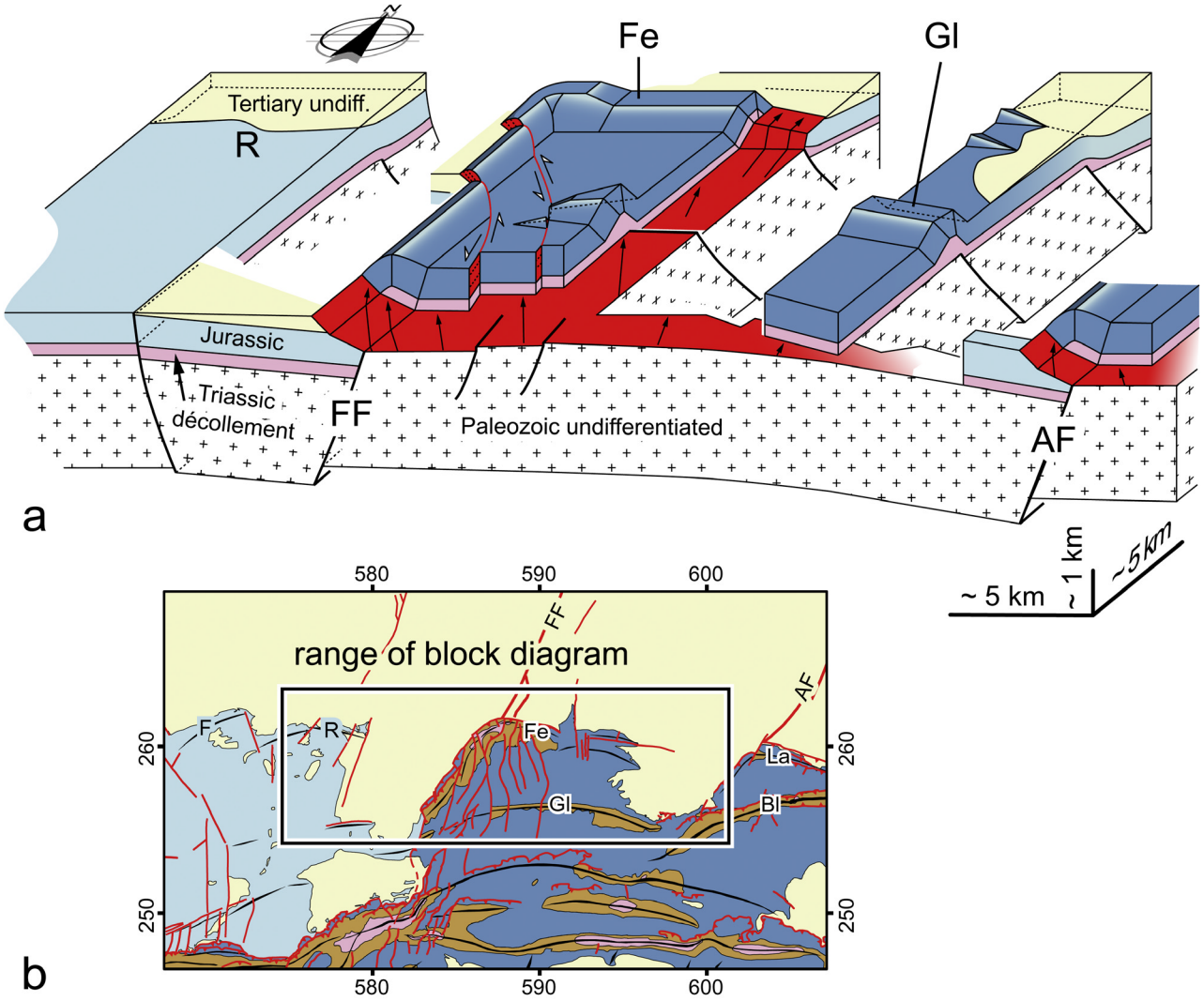

Figure 18. (a) Simplified block diagram illustrating the main tectonic features of the thin-skinned Ferrette Jura and the role of preexisting basement faults, disregarding erosion. Effects of thick-skinned, post-late Pliocene tectonics are not shown. Faults active during the deformation are depicted in red, whereas inactive faults are in black. Black arrows along the basal décollement plane depict displacement directions. The pronounced along-strike asymmetries result from differently oriented basement faults, which control the along-strike change from a NNE trending oblique ramp (above a Paleogene graben) to a frontal ramp (above an E-W trending, formerly extensional flexure). The axial plunge of the Ferrette anticline beneath the Tertiary infill results from an inherited half graben geometry as well as from eastward decrease of the shortening amount. (b) Approximate range of the block diagram. Labeling corresponds to previous figures.

basal décollement and (2) ongoing tectonic underplating in the foreland of the northwestern Alps [*Mosar*, 1999].

[44] 1. The theory that décollement in the Jura fold-and-thrust belt occurred by viscous flow by processes such as intracrystalline glide within the Mid and Upper Triassic halite and anhydrite layers is rheologically viable and widely accepted nowadays [*Laubscher*, 1961; *Müller and Briegel*, 1980; *Jordan*, 1987]. Intracrystalline glide processes in evaporites can be activated at very low temperatures that are equivalent to an overburden column in the order of 1 km. On the basis of apatite fission track data, 1–3 km of uplift and erosion of the entire Swiss Molasse Basin after 5 Ma were recently documented [*Cederbom et al.*, 2004]. According to these authors, the uplift was triggered by accelerated erosion in the Swiss Alps in response to increased precipitation rates, leading to the isostatic rebound of the Alps together with the northerly adjacent foreland basin. It is believed that such an amount of erosion in the northern Molasse Basin may have caused the sedimentary overburden (and, hence, the temperature) to fall beneath a critical threshold necessary to keep intracrystalline glide systems in the basal Jura décollement active. The age of the

uplift is moreover in agreement with the minimum age of thin-skinned folding in the northern Jura Mountains, which predates the onset of sedimentation of the Pliocene Sundgau gravels at 4.2 Ma (see section 2.5).

[45] 2. A crustal-scale transect across the northwestern Alps, including the Molasse Basin and the Jura fold-and-thrust belt, exhibits a steep basal frontal thrust below the external massifs and a very narrow frontal portion [*Mosar*, 1999], an overall geometry that is believed to be unstable when analyzed in terms of the critical taper theory [*Chappel*, 1978; *Davis et al.*, 1983; *Dahlen and Suppe*, 1988]. By integrating geodetically determined uplift rates and the seismicity distribution, *Mosar* [1999] proposed that the Alpine orogenic wedge is currently in the process of accreting new basement nappes from the European crust at its base (below the Jura-Molasse transition) in an attempt to regain stability. If true, the propagation of such incipient thrust faults toward the foreland has conceivably already reached the area of the external Jura fold-and-thrust belt, as revealed by the reverse faulting mechanism of the Mw = 4.5 earthquake in the RBTZ on 23 February 2004, which was rooted in the basement with a focal depth of ~10 km [*Swiss Seismological Service*, 2004].

5. Conclusions

[46] The late Miocene to early Pliocene formation of the thin-skinned Jura fold-and-thrust belt involved the migration of the deformation front far into the Alpine foreland. As the deformation front advanced into the area of the southern URG, it encountered a rift-related structural pattern that had disrupted the Middle and Upper Triassic basal décollement. Preexisting basement faults served as nucleation points for thrust faults and oblique ramps in the detached sedimentary cover. Whereas east to ENE trending normal faults and extensional flexures that delimit an extensive Paleozoic trough system in the subsurface have localized frontal thrusts and anticlines, NNE trending normal faults have localized sinistral oblique ramps. These NNE trending oblique ramps, along which the deformation front of the folded Jura was sinistrally transferred to the north, are characterized by (1) acute angles between the shortening directions and anticline strike, (2) transpressive deformation, and (3) conspicuously dragged anticlines and faults across the NNE trending faults, all indicative of a left-lateral sense of movement. The observed northward fanning of shortening directions obtained from fault slip analysis can be explained by the along-strike decrease of shortening from west to east at the frontal anticline, which necessitated a gentle clockwise rotation of the detached sediments.

[47] Despite the fact that no detectable stress field change occurred in the sedimentary cover, a geodynamic reorganization must have taken place after the late Pliocene. This reorganization apparently led to the deactivation of the basal décollement in the Triassic and (subsequently or simultaneously) to the compressive inversion of formerly extensional basement faults in the Alpine foreland. It is speculated that one or a combination of the following factors might have induced this change: (1) post-5 Ma uplift of the Molasse Basin and concomitant erosion of 1–3 km of its Tertiary infill [*Cederbom et al.*, 2004] (this erosion lowered the overburden that is necessary to keep (thermally induced) intracrystalline glide in the basal décollement active below a critical threshold) and (2) ongoing tectonic underplating of European crust in the foreland of the northwestern Alps [*Mosar*, 1999].

[48] **Acknowledgments.** Marc Schaming (EOST Strasbourg) is thanked for greatly facilitating access to seismic data. Seismic data is the courtesy of Enterprise Oil. Luc Braillard (Université Fribourg) is kindly thanked for providing fault slip data from his ongoing Ph.D. project. This study is a contribution to the EUCOR-URGENT (Upper Rhine Graben Evolution and Neotectonics) project and benefited from logistic and financial support by the European Union-funded ENTEC (Environmental Tectonics) research and training network. We particularly acknowledge financial funding for K.U. by Swiss grant BBW 99-0567-1. We also thank all colleagues from the EUCOR-URGENT team in Basel, particularly Peter Ziegler and Pierre Dèzes, for many fruitful discussions and their ongoing support. An anonymous reviewer's constructive comments helped in finalizing the manuscript.

References

Affolter, T., and J. Gratier (2004), Map view retrodeformation of an arcuate fold-and-thrust belt: The Jura case, *J. Geophys. Res.*, *109*, B03404, doi:10.1029/2002JB002270.

Anderson, E. M. (1951), *The Dynamics of Faulting and Dyke Formation With Applications to Britain*, 206 pp., Oliver and Boyd, White Plains, N. Y.

Angelier, J., and P. Mechler (1977), Sur une méthode graphique de recherche des contraintes principales également utilisable en tectonique et en seismologie: La méthode des dièdres droits, *Bull. Soc. Geol. Fr.*, *19*, 1309–1318.

Becker, A. (2000), The Jura Mountains: An active foreland fold-and-thrust belt?, *Tectonophysics*, *321*, 381–406.

Bolliger, T., B. Engesser, and M. Weidmann (1993), Première découverte de mammifères pliocènes dans le Jura Neuchâtelois, *Eclogae Geol. Helv.*, *86*, 1031–1068.

Braillard, L. (2006), Morphogenèse des vallées sèches du Jura tabulaire d'Ajoie (Suisse) - rôle de la fracturation et étude des remplissages quaternaires, in *Geofocus*, Univ. de Fribourg, Fribourg, Switzerland, in press.

Burkhard, M., and A. Sommaruga (1998), Evolution of the western Swiss Molasse basin: Structural relations with the Alps and the Jura belt, in *Cenozoic Foreland Basins of Western Europe*, edited by A. Mascle et al., *Geol. Soc. Spec. Publ.*, *134*, 279–298.

Cederbom, C. E., H. D. Sinclair, F. Schlunegger, and M. Rahn (2004), Climate-induced rebound and exhumation of the European Alps, *Geology*, *32*, 709–712, doi:10.1130/G20491.1.

Chappel, W. M. (1978), Mechanics of thin-skinned fold-and-thrust belts, *Geol. Soc. Am. Bull.*, *89*, 1189–1198.

Dahlen, F. A., and J. Suppe (1988), Mechanics, growth and erosion of mountain belts, in *Processes in Continental Lithospheric Deformation*, edited by S. P. Clark, B. C. Burchfiel, and J. Suppe, *Spec. Pap. Geol. Soc. Am.*, *218*, 161–178.

Dannecker, P. (1995), Tektonik des Pfirter Jura, Diploma thesis, 62 pp., Univ. Karlsruhe, Karlsruhe, Germany.

Davis, D., J. Suppe, and F. A. Dahlen (1983), Mechanics of fold-and-thrust belts and accretionary wedges, *J. Geophys. Res.*, *88*, 1153–1172.

Deichmann, N., D. Ballarin Dolfin, and U. Kastrup (2000), Seismizität der Nord- und Zentralschweiz, *NAGRA Tech. Ber. NTB 00-05*, 94 pp., Natl. Assoc. for the Storage of Nucl. Waste, Wettingen, Germany.

Delvaux, D., R. Moeys, G. Stapel, C. Petit, K. Levi, A. Miroshnichenko, V. Ruzhich, and V. San'kov (1997), Paleostress reconstruction and geodynamics of the Baykal region, *Tectonophysics*, *282*, 1–38.

Dèzes, P., S. M. Schmid, and P. A. Ziegler (2004), Evolution of the European Cenozoic Rift System: Interaction of the Alpine and Pyrenean orogens with their foreland lithosphere, *Tectonophysics*, *389*, 1–33.

Diebold, P., H. Laubscher, A. Schneider, and R. Tschopp (1963), Geologischer Atlas der Schweiz, Atlasblatt 40, St. Ursanne, mit Erläuterungen, Schweiz. Geol. Komm., Bern.

Fischer, H. (1965), *Geologie des Gebietes zwischen Blauen und Pfirter Jura (SW Basel)*, 106 pp., Geogr. Verlag, Bern.

Gehring, A. U., P. Keller, and F. Heller (1991), Paleomagnetism and tectonics of the Jura arcuate mountain belt in France and Switzerland, *Tectonophysics*, *186*, 269–278.

Giamboni, M., K. Ustaszewski, S. M. Schmid, M. E. Schumacher, and A. Wetzel (2004), Plio-Pleistocene transpressional reactivation of Paleozoic and Paleogene structures in the Rhine-Bresse transform zone (northern Switzerland and eastern France), *Int. J. Earth Sci.*, *93*, 207–223, doi:10.1007/s00531-003-0375-2.

Hancock, P. L. (1985), Brittle microtectonics: Principles and practice, *J. Struct. Geol.*, *7*, 437–457.

Hindle, D., and M. Burkhard (1999), Strain, displacement and rotation associated with the formation of curvature in fold belts; the example of the Jura arc, *J. Struct. Geol.*, *21*, 1089–1101.

Hug, W. A., J. P. Berger, I. Clément, D. Kälin, and M. Weidmann (1997a), Miocene fossiliferous paleokarst (MN4) and OSM deposits (MN5–?) near Glovelier (Swiss Jura Mountains), paper presented at Fifth Meeting of Swiss Sedimentologists (SwissSed) and Meeting of Molasse Group, Fribourg, Switzerland.

Hug, W. A., J. P. Berger, I. Clément, D. Kälin, and M. Weidmann (1997b), Sedimentological history of a Miocene fossiliferous paleokarst near Glovelier (Swiss Jura Mountains), paper presented at 18th IAS Regional European Meeting of Sedimentology, Int. Assoc. of Sedimentol., Heidelberg, Germany.

Jordan, P. (1987), Eine Methode zur Abschätzung tektonischer Scherraten aufgrund mikrostruktureller Beobachtungen, *Eclogae Geol. Helv.*, *80*, 491–508.

Kälin, D. (1997), Litho- und Biostratigraphie der mittel- bis obermiozänen Bois de Raube-Formation (Nordwestschweiz), *Eclogae Geol. Helv.*, *90*, 97–114.

Kastrup, U., M. L. Zoback, N. Deichmann, K. F. Evans, D. Giardini, and A. J. Michael (2004), Stress field variations in the Swiss Alps and the northern Alpine foreland derived from inversion of fault plane solutions, *J. Geophys. Res.*, *109*, B01402, doi:10.1029/2003JB002550.

Kemna, H. A., and R. Becker-Haumann (2003), Die Wanderblock-Bildungen im Schweizer Juragebirge südlich von Basel: Neue Daten zu einem alten Problem, *Eclogae Geol. Helv.*, *96*, 71–84.

Larroque, J.-M., and P. Laurent (1988), Evolution of the stress field pattern in the south of the Rhine Graben from the Eocene to the present, *Tectonophysics*, *148*, 41–58.

Laubscher, H. (1961), Die Fernschubhypothese der Jurafaltung, *Eclogae Geol. Helv.*, *54*, 222–282.

Laubscher, H. (1972), Some overall aspects of Jura dynamics, *Am. J. Sci.*, *272*, 293–304.

Laubscher, H. (1977), Fold development in the Jura, *Tectonophysics*, *37*, 337–362.

Laubscher, H. (1981), The 3D propagation of décollement in the Jura, in *Thrust and Nappe Tectonics*, edited by K. R. McClay and N.J. Price, *Geol. Soc. Spec. Publ.*, *9*, 311–318.

Laubscher, H. (1986), The eastern Jura: Relations between thin-skinned and basement tectonics, local and regional, *Geol. Rundsch.*, *75*, 535–553.

Laubscher, H. (1987), Die tektonische Entwicklung der Nordschweiz, *Eclogae Geol. Helv.*, *80*, 287–303.

Laubscher, H. (1992), Jura kinematics and the Molasse Basin, *Eclogae Geol. Helv.*, *85*, 653–675.

Laubscher, H. (2001), Plate interactions at the southern end of the Rhine graben, *Tectonophysics*, *343*, 1–19.

Laubscher, H. (2003), The Miocene dislocations in the northern foreland of the Alps: Oblique subduction and its consequences (Basel area, Switzerland-Germany), *Jahresber. Mitt. Oberrheinischen Geol. Vereins*, *85*, 423–439.

Liniger, H. (1970), Geologischer Atlas der Schweiz 1:25 000, Atlasblatt 55: Bonfol, mit Erläuterungen, Kümmerly and Frey, Bern.

Lopes Cardozo, G. G. O., and M. Granet (2003), New insight in the tectonics of the southern Rhine Graben-Jura region using local earthquake seismology, *Tectonics*, *22*(6), 1078, doi:10.1029/2002TC001442.

Marrett, R., and R. W. Allmendinger (1990), Kinematic analysis of fault-slip data, *J. Struct. Geol.*, *12*, 973–986.

Meier, D. (1984), Zur Tektonik des schweizerischen Tafel- und Faltenjura (regionale und lokale Strukturen, Kluftgenese, Bruch- und Faltentektonik, Drucklösung), *Clausthaler Geowiss.*, 14.

Meyer, B., R. Lacassin, J. Brulhet, and B. Mouroux (1994), The Basel 1356 earthquake: Which fault produced it?, *Terra Nova*, *6*, 54–63.

Mosar, J. (1999), Present-day and future tectonic underplating in the western Swiss Alps: Reconciliation of basement/wrench-faulting and décollement folding of the Jura and Molasse basin in the Alpine foreland, *Earth Planet. Sci. Lett.*, *173*, 143–155.

Müller, W. H., and U. Briegel (1980), Mechanical aspects of the Jura overthrust, *Eclogae Geol. Helv.*, *73*, 239–250.

Nivière, B., and T. Winter (2000), Pleistocene northwards fold propagation of the Jura within the southern Upper Rhine Graben: Seismotectonic implications, *Global Planet. Change*, *27*, 263–288.

Noack, T. (1995), Thrust development in the eastern Jura Mountains related to pre-existing extensional structures, *Tectonophysics*, *252*, 419–431.

Petit, C., M. Campy, J. Chaline, and J. Bonvalot (1996), Major palaeohydrographic changes in Alpine foreland during the Pliocene-Pleistocene, *Boreas*, *25*, 131–143.

Petit, J. P. (1987), Criteria for the sense of movement on fault surfaces in brittle rocks, *J. Struct. Geol.*, *9*, 597–608.

Pfiffner, O. A., and M. Burkhard (1987), Determination of paleo-stress axes orientations from fault, twin and earthquake data, *Ann. Tectonicae*, *1*, 48–57.

Philippe, Y. (1994), Transfer zone in the southern Jura Thrust Belt (eastern France): Geometry, Development and comparison with analogue modeling experiments, in *Hydrocarbon and Petroleum Geology of France*, edited by A. Mascle, *Spec. Publ. Eur. Assoc. Pet. Geol.*, *4*, 327–346.

Philippe, Y. (1995), Rampes latérales et zones de transfert dans les chãcirc;nes plissées: Géometrie, conditions de formation et pièges structuraux associés, Ph.D. thesis, 272 pp., Univ. de Savoie and Inst. Fr. du Pét., Paris.

Philippe, Y., B. Colletta, E. Deville, and A. Mascle (1996), The Jura fold-and-thrust belt: A kinematic model based on map-balancing, in *Peri-Tethys Memoir 2: Structure and prospects of Alpine Basins and Forelands.*, edited by P. Ziegler and F. Horvath, *Mem. Mus. Nat. Hist. Nat.*, *170*, 235–261.

Plenefisch, T., and K. Bonjer (1997), The stress field in the Rhine Graben area inferred from earthquake focal mechanisms and estimation of frictional parameters, *Tectonophysics*, *275*, 71–97.

Plessmann, W. (1972), Horizontal-Stylolithen im französisch-schweizerischen Tafel- und Faltenjura und ihre Einpassung in den regionalen Rahmen, *Geol. Rundsch.*, *61*, 332–347.

Reinecker, J., O. Heidbach, and B. Mueller (2003), The 2003 release of the World Stress Map, World Stress Map Proj., Heidelberg Acad. of Sci. and Humanities, Heidelberg, Germany. (Available at http://www.world-stress-map.org)

Reiter, F., and P. Acs, (1996–2000), Computer Software for Structural Geology, version 2.0 PR, TectonicsFP, Innsbruck. (Available at http://www.tectonicsfp.com/)

Ruhland, M., J. G. Blanalt, and M. Bômont (1973), Carte Géologique détaillée de la France à 1/50 000, Ferrette, feuille XXXVII-22, Ministère du développement industriel et scientifique, Bureau de Rech. Géol. et Minièr., Serv. Géol. Natl., Orléans, France.

Schmid, S. M., O. A. Pfiffner, N. Froitzheim, G. Schönborn, and E. Kissling (1996), Geophysical-geological transect and tectonic evolution of the Swiss-Italian Alps, *Tectonics*, *15*, 1036–1064.

Schneegans, D., and N. Théobald (1948), Observations nouvelles sur le Chevauchement frontal du Jura Alsacien, *Bull. Soc. Geol. Fr.*, *18*, 89–95.

Schneegans, D., N. Théobald, W. T. Keller, and A. Werenfels (1934), Carte géologique de la France à l'échelle du 1/50 000, sheet Ferrette 37-21, Serv. de la Carte Géol. d'Alsace et de Lorraine, Strasbourg, France.

Schumacher, M. E. (2002), Upper Rhine Graben: Role of preexisting structures during rift evolution, *Tectonics*, *21*(1), 1006, doi:10.1029/2001TC900022.

Sperner, B., and L. Ratschbacher (1994), A Turbo Pascal program package for graphical presentation and stress analysis of calcite deformation, *Z. Dtsch. Geol. Ges.*, *145*, 414–423.

Steininger, F. F., W. A. Berggren, D. V. Kent, R. L. Bernor, S. Sen, and J. Agusti (1996), Circum-Mediterranean Neogene (Miocene and Pliocene) marine-continental chronologic correlations of European Mammal Units, in *The Evolution of Western Eurasian Neogene Mammal Faunas*, edited by R. L. Bernor, V. Fahlbusch, and H.-W. Mittmann, pp. 7–46, Columbia Univ. Press, New York.

Swiss Seismological Service (2004), Regional moment tensor catalog, ETH Zürich, Zürich. (Available at http://www.seismo.ethz.ch/moment_tensor/2004/homepage.html)

Théobald, N., G. Dubois, and J. Goguel (1958), Carte Géologique de la France à 1/50 000, sheet Altkirch-Huningue and explanatory leaflet, 37–21, Serv. de la Carte Géol. de la Fr., Paris.

Ustaszewski, K. (2004), Reactivation of pre-existing crustal discontinuities: The southern Upper Rhine Graben and the northern Jura Mountains—A natural laboratory, Ph.D. thesis, 162 pp., Univ. of Basel, Basel, Switzerland.

Ustaszewski, K., M. E. Schumacher, and S. M. Schmid (2005a), Simultaneous normal faulting and extensional flexuring during rifting: An example from the southernmost Upper Rhine Graben, *Int. J. Earth Sci.*, *94*, 680–696, doi:10.1007/s00531-004-0454-z.

Ustaszewski, K., M. E. Schumacher, S. M. Schmid, and D. Nieuwland (2005b), Fault reactivation in brittle-viscous wrench systems—Dynamically scaled analogue models and application to the Rhine-Bresse Transfer Zone, *Quat. Sci. Rev.*, *24*, 363–380, doi:10.1016/j.quascirev.2004.03.015.

Ziegler, P. A. (1992), European Cenozoic rift system, *Tectonophysics*, *208*, 91–111.

Ziegler, P. A., M. E. Schumacher, P. Dèzes, J.-D. van Wees, and S. Cloetingh (2004), Post-Variscan evolution of the lithosphere in the Rhine Graben area: Constraints from subsidence modelling, in *Permo-Carboniferous Magmatism and Rifting in Europe*, edited by M. Wilson, *Geol. Soc. Spec. Publ.*, *223*, 289–317.

S. M. Schmid and K. Ustaszewski, Geologisch-Paläontologisches Institut, University Basel, Bernoullistrasse 32, CH-4056 Basel, Switzerland. (kamil.ustaszewski@unibas.ch)